

AD-A091 908

HARRY DIAMOND LABS ADELPHI MD  
A NEAR-SURFACE BURST EMP DRIVER PACKAGE FOR NEUTRON-INDUCED SOU--ETC(U)  
SEP 80 W T WYATT  
HOL-TR-1930

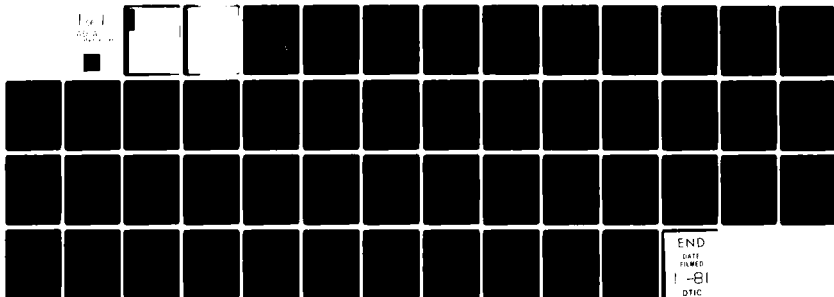
F/G 18/3

UNCLASSIFIED

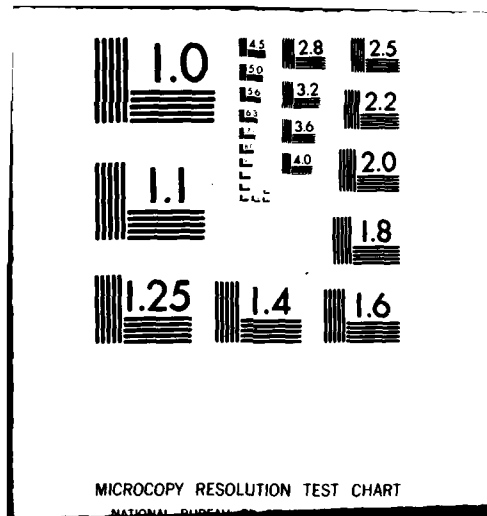
NL

Doc  
ID: A091 908

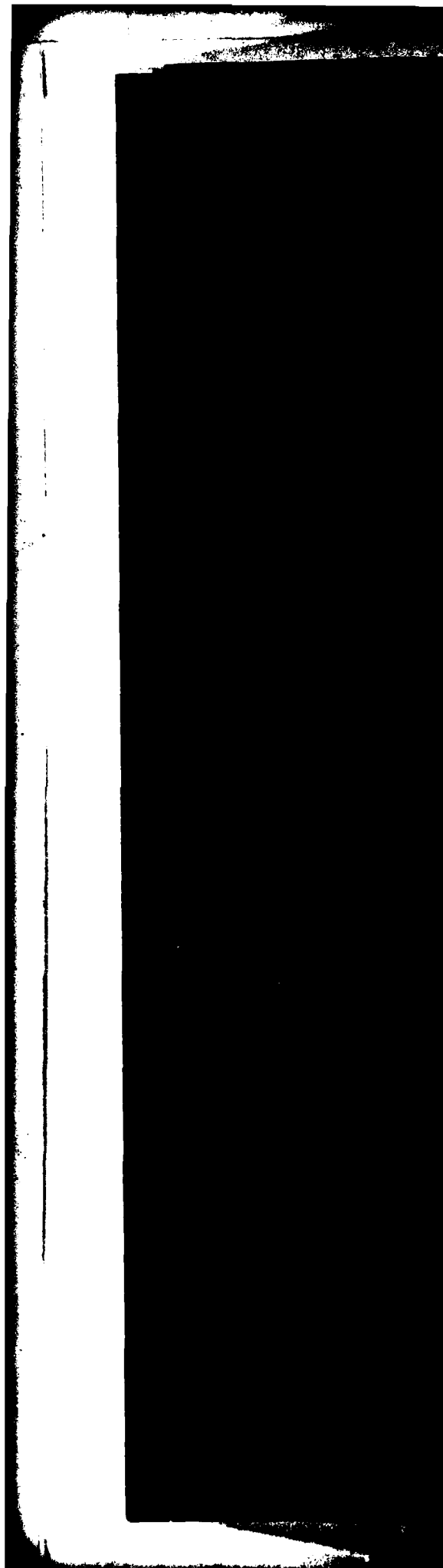
■



END  
DATE  
FILMED  
1-81  
DTIC



AD A091908



UNCLASSIFIED

SECURITY CLASSIFICATION OF THIS PAGE (When Data Entered)

REPORT DOCUMENTATION PAGE		READ INSTRUCTIONS BEFORE COMPLETING FORM
1. REPORT NUMBER HDL-TR-1936/	2. GOVT ACCESSION NO. AD A091908	3. RECIPIENT'S CATALOG NUMBER 9
4. TITLE (and Subtitle) A Near-Surface Burst EMP Driver Package for Neutron-Induced Sources.		5. TYPE OF REPORT & PERIOD COVERED Technical Report.
7. AUTHOR(s) William T. Wyatt, Jr.		6. PERFORMING ORG. REPORT NUMBER
8. PERFORMING ORGANIZATION NAME AND ADDRESS Harry Diamond Laboratories 2800 Powder Mill Road Adelphi, MD 20783		9. CONTRACT OR GRANT NUMBER(s)
10. CONTROLLING OFFICE NAME AND ADDRESS U.S. Army Materiel Development and Readiness Command Alexandria, VA 22333		10. PROGRAM ELEMENT, PROJECT, TASK AREA & WORK UNIT NUMBERS Prog. El.: 6.21.20.A
11. MONITORING AGENCY NAME & ADDRESS (if different from Controlling Office) 12/52		11. REPORT DATE September 1980
		12. NUMBER OF PAGES 50
		13. SECURITY CLASS. (of this report) UNCLASSIFIED
		13a. DECLASSIFICATION/DOWNGRADING SCHEDULE
14. DISTRIBUTION STATEMENT (of this Report) Approved for public release; distribution unlimited.		
15. DISTRIBUTION STATEMENT (of the abstract entered in Block 20, if different from Report)		
16. SUPPLEMENTARY NOTES HDL Project: X759E6 DRCMS Code: 612120.H.250011 DA Project: 1L162120AH25 16		
17. KEY WORDS (Continue on reverse side if necessary and identify by block number) EMP Curve fitting Compton currents Minimization Ionization Numerical integration Nuclear explosions Electromagnetic pulse Radiation transport		
18. ABSTRACT (Continue on reverse side if necessary and identify by block number) This report describes the development of a software package developed for the NEMP computer code, specifying time- and space-dependent drivers produced by neutrons emitted from a near-surface nuclear detonation in the air. Well-chosen functionals were fitted to previously obtained Monte Carlo transport results. The fit was done globally to all volume detectors and time bins together for each driver. Highly efficient minimization algorithms were employed to obtain each fit. Separate drivers for radial and		

DD FORM 1 JAN 75 1473 EDITION OF 1 NOV 65 IS OBSOLETE

UNCLASSIFIED

SECURITY CLASSIFICATION OF THIS PAGE (When Data Entered)

1

163050

DTIC  
NOV 21 1980  
C

&gt; over

Ym

UNCLASSIFIED

SECURITY CLASSIFICATION OF THIS PAGE(When Data Entered)

2004 → theta Compton currents and for ionization rate were determined for nine source neutron energy bands, for five classes of neutron interaction including (1) neutron direct ionization by elastic recoil and charged particle production, and secondary gamma production by (2) high energy air reactions, (3) low energy air reactions, (4) high energy ground reactions, and (5) low energy ground reactions. Burst height dependence of the drivers was determined. Comparisons with experiment and previous theory are briefly discussed. Typical driver results are presented and discussed. The package allows flexible representation of any nuclear weapon neutron energy spectrum and choice of any burst height in the near-surface regime.

A

Accession For	
NTIS GRA&I	<input checked="checked" type="checkbox"/>
DTIC TAB	<input type="checkbox"/>
Unannounced	<input type="checkbox"/>
Justification	
By _____	
Distribution/	
Availability Codes	
Dist	Avail and/or Special
A	

UNCLASSIFIED

## CONTENTS

	<u>Page</u>
1. INTRODUCTION.....	5
2. MOTIVATION.....	5
3. APPROACH.....	8
4. CURVE-FITTING PROCEDURE.....	8
5. MINIMIZATION OF FIT ERROR.....	12
6. BURST HEIGHT DEPENDENCE OF FIT PARAMETERS.....	20
7. COMPARISON WITH LIQUID AIR EXPERIMENT.....	21
8. COMPARISON WITH EARLIER APPROXIMATION FOR IONIZATION BY 14-MeV NEUTRONS.....	22
9. SELECTED RESULTS.....	23
10. CONCLUSIONS.....	31
LITERATURE CITED.....	33
DISTRIBUTION.....	45

## APPENDICES

A.--A TWO-POINT QUADRATURE SCHEME.....	35
B.--DESCENT ALGORITHMS USED.....	39

## FIGURES

1 Fitting algorithm.....	12
2 Radial Compton current for 1-m burst height, 0-m observer height, and 1000-m ground range.....	25
3 Theta Compton current for 1-m burst height, 0-m observer height, and 1000-m ground range.....	26
4 Ionization rate for 1-m burst height, 0-m observer height, and 1000-m ground range.....	26

## CONTENTS (Cont'd)

	<u>Page</u>
5 Radial Compton current for 1-m burst height, 500-m observer height, and 1000-m ground range.....	27
6 Theta Compton current for 1-m burst height, 500-m observer height, and 1000-m ground range.....	27
7 Ionization rate for 1-m burst height, 500-m observer height, and 1000-m ground range.....	28
8 Radial Compton current for 200-m burst height, 0-m observer height, and 1000-m ground range.....	28
9 Theta Compton current for 200-m burst height, 0-m observer height, and 1000-m ground range.....	29
10 Ionization rate for 200-m burst height, 0-m observer height, and 1000-m ground range.....	29
11 Radial Compton current for 200-m burst height, 500-m observer height, and 1000-m ground range.....	30
12 Theta Compton current for 200-m burst height, 500-m observer height, and 1000-m ground range.....	30
13 Ionization rate for 200-m burst height, 500-m observer height, and 1000-m ground range.....	31

## TABLES

1 Monte Carlo Data Characteristics.....	7
2 Effect of Minimizing Penalty Function for Ionization Rate.....	19



## 1. INTRODUCTION

Various Army electronic systems may be exposed to nuclear explosion effects in a tactical battlefield. Included among these nuclear effects is the nuclear electromagnetic pulse (EMP), which is a transient broadband electromagnetic field capable of damaging or upsetting electronic equipment. To predict the signature of the EMP generated by a nuclear burst, it is necessary to determine the physical parameters that induce the EMP. These parameters, called EMP drivers, are time and space varying ionization and Compton electron currents in the nuclear radiation field around the burst. Once the ionization and the currents are specified, it is usually possible to solve some form of Maxwell's equations for the EMP generated. This report summarizes the development of a software package specifying EMP drivers produced by neutrons emitted from a near-surface burst in the air. The package was designed for use with the NEMP computer code used at the Harry Diamond Laboratories (HDL). A separate report<sup>1</sup> summarizes the development of a similar software package for EMP drivers due to prompt gamma radiation.

## 2. MOTIVATION

The EMP drivers are due to one component arising from prompt gamma radiation and a second component arising from neutron radiation. The neutron component includes elastic recoil ionization (frequently called "heating") by air constituent nuclei and also includes effects of secondary gamma radiation produced by a number of neutron capture and inelastic collision reactions in the air and the ground. The development of EMP drivers by secondary gamma rays is physically similar to the development for prompt gamma radiation, although the magnitude, the direction, and the time dependence are markedly different.

Maxwell's equations for EMP from a near-surface burst are solved by the NEMP computer code.<sup>2,3</sup> The NEMP code requires EMP drivers to be specified in a volume extending to several kilometers from the burst point and for times extending to many milliseconds after the instant of burst. The EMP drivers must be incorporated into the code as smooth fits to results of quasi-analytic or Monte Carlo predictions. The NEMP

---

<sup>1</sup>William T. Wyatt, Jr., *A Near-Surface Burst EMP Driver Package for Prompt Gamma-Induced Sources*, Harry Diamond Laboratories HDL-TR-1931 (1980).

<sup>2</sup>H. J. Longley, C. L. Longmire, and K. S. Smith, *Development of NEMP (U)*, Mission Research Corp., Santa Barbara, CA, HDL-CR-75-001-1 (April 1975). (SECRET--RESTRICTED DATA)

<sup>3</sup>H. J. Longley and K. S. Smith, *Developments in NEMP for 1977 (U)*, Mission Research Corp., Santa Barbara, CA, HDL-CR-77-0022-1 (January 1978). (SECRET--RESTRICTED DATA)

code in many respects is an extension of the LEMP computer code<sup>4</sup> for EMP from surface bursts, which was initially developed from about 1966 to about 1969. The EMP drivers in the earlier LEMP code could have been modified and used in the NEMP code with certain limitations. These limitations are discussed briefly, and reasons are given for the importance of the new results reported here.

In this study, the neutron-induced EMP drivers are divided into five categories: (1) neutron elastic (recoil) ionization, (2) fast neutron air inelastic collision ( $n, n'\gamma$ ) drivers (both Compton electron currents and ionization), (3) fast neutron ground inelastic collision ( $n, n'\gamma$ ) and capture ( $n, \gamma$ ) drivers, (4) thermal neutron ground capture ( $n, \gamma$ ) drivers, and (5) thermal neutron air capture ( $n, \gamma$ ) drivers. Of these, one would expect the NEMP geometry to introduce complications to LEMP code prescriptions for categories (1), (2), and (4), since the proximity of the ground is different. Category (5) was not treated originally by the LEMP code. Category (3) would be quite different for the NEMP code and probably of reduced magnitude. However, the cross sections for most of the above reactions have been subjected to concentrated study and revision with the advent of the Evaluated Nuclear Data File (ENDF-B, distributed Brookhaven National Laboratory, Brookhaven, NY). It is likely that new neutron transport studies based on recent ENDF-B cross sections would produce results different from those upon which the LEMP code neutron-induced EMP drivers were based. Further, by omission of the thermal neutron air capture ( $n, \gamma$ ) drivers, the LEMP drivers were limited to times less than about 1 ms after the burst.

The LEMP authors<sup>5</sup> developed a newer and much more complete prescription of categories (1) through (5) based on results of Sargis and others.<sup>6</sup> Factors weighing against the use of these prescriptions in the NEMP code include the following: First, a newer revision (Round 3) of ENDF-B was released in 1973. Second, the only burst heights considered by Sargis were 0, 200, and 500 m, whereas the NEMP code operates principally at tactical burst heights between 0 and 200 m. Third, the new LEMP EMP driver curve fits were considered by this writer to neglect certain important ground-air interface effects such as time-dependent depletion and enhancement. Fourth, the transport results<sup>6</sup> were based on

---

<sup>4</sup>H. J. Longley and C. L. Longmire, Development and Testing of LEMP 1, Los Alamos Scientific Laboratory, NM, LA-4346 (April 1970).

<sup>5</sup>H. J. Longley, C. L. Longmire, J. S. Malik, R. M. Hamilton, R. N. Marks, and K. S. Smith, Development and Testing of LEMP 2, A Surface Burst EMP Code (U), Mission Research Corp., Santa Barbara, CA, DNA 4097T (December 1976). (CONFIDENTIAL)

<sup>6</sup>D. A. Sargis, E. R. Parkinson, J. N. Wood, R. E. Dietz, and C. A. Stevens, Late-Time Sources for Close-In EMP, Science Applications, Inc., La Jolla, CA, DNA 3064F (August 1972).

"energy grouped" cross sections, whereas a "point" cross-section treatment should be more accurate at deep penetrations. Fifth, a single typical source neutron energy spectrum was used in the LEMP drivers, with a parameter available for adjusting the concentration of high-energy (14-MeV) neutrons; a more desirable package would allow flexible representation of arbitrary source neutron energy spectra.

For these reasons, new Monte Carlo transport calculations have been done to describe more accurately the neutron-induced EMP drivers.<sup>7</sup> The extent of these calculations is summarized in table 1. Edited results of these calculations were transmitted to this writer on computer magnetic tape and used to derive the EMP driver software package reported here.

TABLE 1. MONTE CARLO DATA CHARACTERISTICS

Source neutron energy band (MeV)	Time bin boundary (s)	Burst height (m)	EMP driver
0.0 to 0.11	0.0 to 1.0(-7)*	1	Neutron direct ionization
0.11 to 0.55	1.0(-7) to 2.15(-7)	50	High-energy air, radial current
0.55 to 1.11	2.15(-7) to 4.64(-7)	100	High-energy air, theta current
1.11 to 1.83	4.64(-7) to 1.0(-6)	200	High-energy air, ionization
1.83 to 2.35	1.0(-6) to 2.15(-6)		Low-energy air, radial current
2.35 to 4.07	2.15(-6) to 4.64(-6)		Low-energy air, theta current
4.07 to 6.36	4.64(-6) to 1.0(-5)		Low-energy air, ionization
6.36 to 8.19	1.0(-5) to 2.15(-5)		High-energy ground, radial current
8.19 to 15.0	2.15(-5) to 4.64(-5)		High-energy ground, theta current
	4.64(-5) to 1.0(-4)		High-energy ground, ionization
	1.0(-4) to 2.15(-4)		Low-energy ground, radial current
	2.15(-4) to 4.64(-4)		Low-energy ground, theta current
	4.64(-4) to 1.0(-3)		Low-energy ground, ionization
	1.0(-3) to 2.15(-3)		
	2.15(-3) to 4.64(-3)		
	4.64(-3) to 1.0(-2)		
	1.0(-2) to 2.15(-2)		
	2.15(-2) to 4.64(-2)		
	4.64(-2) to 1.0(-1)		

\*Read as  $1.0 \times 10^{-7}$ .

<sup>7</sup>H. S. Schechter and M. O. Cohen, *Energy Deposition Rates and Compton Electron Currents from Low-Altitude Bursts as a Function of Source Energy*, Mathematical Applications Group, Inc., Elmsford, NY, HDL-CR-77-020-1 (November 1977).

### 3. APPROACH

The edited results of Monte Carlo calculations contain statistical fluctuations inherent in the Monte Carlo method. The NEMP code demands smooth prescriptions of the EMP drivers to obtain useful results. One may attempt to fit smooth general functions (such as polynomials) to the Monte Carlo results by a least-squares fitting technique, for example, or one may attempt to fit the Monte Carlo results with certain appropriate smooth functional forms. By using a polynomial of sufficiently high degree, the former technique may allow the Monte Carlo results to be fitted more faithfully than the latter, but the closer fit may mean that the "noise" is being fitted instead of the underlying smooth "true answer." The same difficulty can arise by using the latter technique if too many degrees of freedom are permitted. On the other hand, if the polynomial degree is not high enough, the fit may be a poor representation of the true answer. In general, however, using appropriate smooth functional forms will involve far fewer degrees of freedom than using general functions if the functional forms are well chosen and if the fit is a global fit over the entire space-time volume of interest rather than a piecewise fit over many smaller subdivisions of the space-time volume.

The strength of the technique of using well-chosen functional forms is that physical variables usually do behave according to relatively simple physical principles that are approximately described by relatively simple functional forms. A global fit of properly chosen functional forms to Monte Carlo results could reduce the error below the statistical error of the Monte Carlo calculation. The fitting algorithm should heavily weight low-variance results over high-variance results to reduce the error.

The new edited Monte Carlo results for neutron-induced EMP drivers consist of three physical quantities (energy deposition and radial and polar components of Compton electron current) defined for 19 time intervals within 63 spatial volume detectors, for five categories of reaction (recoil, air inelastic, etc.), four burst heights, and nine source neutron energy bands (table 1). There are 646,380 quantities to be fitted. Apparently, the fitting algorithm must be highly automated to allow useful results to be obtained with a realistic investment of human effort.

### 4. CURVE-FITTING PROCEDURE

Thirteen distinct functions describe the time and space dependence of 13 EMP drivers:

(1) Ionization in the air from neutron elastic collisions and charged particle production (such as (n,p) and (n, $\alpha$ ) reactions that deposit kinetic energy locally)

(2) Radial Compton electron current in the air (measured in the polar coordinate system centered at the burst) due to high-energy neutron reactions in the air (neutron energy more than 0.1 MeV)

(3) Polar Compton electron current in the air for the same as (2)

(4) Ionization in the air for the same as (2)

(5) Radial Compton electron current in the air due to low-energy neutron reactions in the air (neutron energy less than 0.1 MeV)

(6) Polar Compton electron current in the air for the same as (5)

(7) Ionization in the air for the same as (5)

(8) Radial Compton electron current in the air (measured in the polar coordinate system centered on the ground beneath the burst) due to high-energy neutron reactions in the ground

(9) Polar Compton electron current in the air for the same as (8)

(10) Ionization in the air for the same as (8)

(11) Radial Compton electron current in the air due to low-energy neutron reactions in the ground

(12) Polar Compton electron current in the air for the same as (11)

(13) Ionization in the air for the same as (11)

Drivers (2), (3), and (4) are due principally to high-energy inelastic collisions with atmospheric nitrogen. Drivers (5), (6), and (7) are due to thermal capture by atmospheric nitrogen. Drivers (8), (9), and (10) are due to inelastic collisions with the ground and fast neutron capture by the ground. Drivers (11), (12), and (13) are due to thermal neutron capture by the ground.

A mathematical notation is used to simplify the succeeding discussion. The vector functional  $F$  represents the drivers.  $F$  is dependent on time ( $t$ ) and space ( $x, y, z$ ). Subscript  $d$  running from 1 to 13 denotes which of the drivers is represented:

$$F_d(t, x, y, z)$$

Time  $t$  is the local time, retarded by the speed of light from the coordinate center.

The functional  $F_d$  is a functional form incorporating a certain number,  $n_d$ , of parameters  $p$ . This is written as

$$F_d(t, x, y, z; p_{di}) ,$$

where  $p_{di}$ ,  $i = 1$  to  $n_d$ , is interpreted as the parameter vector of length  $n_d$  for driver  $d$ . In general,  $n_d$  is not the same for different  $d$ , but is approximately 10 in this report.

Parameters  $p_{di}$  are evidently dependent on the energy of the source neutrons producing the drivers and on the height of burst. Other variables are ignored, such as variations in water content of the air and the ground and variations in ground composition. The parameters may then be written

$$p_{di}(j, h)$$

or

$$p_{dij}(h) ,$$

where  $j$  denotes the ordinal of the source neutron discrete energy band and  $h$  is the height of burst. In this way,  $p$  is a discrete function of the source neutron energy (band) and a continuous function of the height of burst. It thus appears that the EMP driver fits

$$F_d(t, x, y, z; p_{dij})$$

are defined when parameters  $p_{dij}$  are evaluated for a specific height of burst,

$$p_{dij} = p_{dij}(h) .$$

The total number of functions  $p_{dij}(h)$  to be determined is

$$\sum_{d=1}^{13} \sum_{i=1}^{n_d} \sum_{j=1}^9 1 = \sum_{d=1}^{13} \sum_{i=1}^{n_d} 9 .$$

Since  $n_d \sim 10$ , this total is roughly 1100. Thus, there are over a thousand such functions to be specified. Determination of this many functions was a formidable undertaking and required considerable computer time (about 40 hr on an IBM System/370 Model 168).

The following strategy was adopted:

a. Through previous experience supported by trial and error, 13 functional forms were constructed to constitute driver functionals  $F_d$ . These were functions of time and space and were based on a certain number,  $n_d$ , of parameters.

b. Monte Carlo predictions for the 13 drivers were available as functions of time for each of 63 spatial volume detectors around the burst for each combination of four burst heights and nine source neutron energy bands. For a particular source neutron energy band, each driver functional was fitted to the time and space dependence of the Monte Carlo data, for each of the four sets of data corresponding to the four heights of burst (1, 50, 100, and 200 m). The fit was obtained through an optimization process by adjustment of each of the  $n_d$  parameters for the driver.

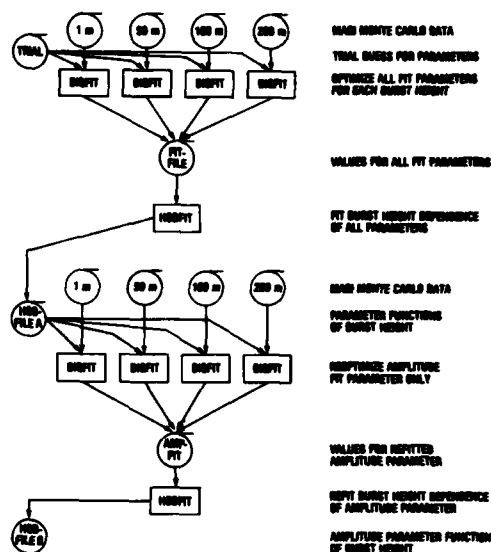
c. Four values,  $\hat{p}_{dij}(h_k)$ ,  $k = 1$  to 4, were thus derived for each parameter  $p_{dij}$  corresponding to the four heights of burst. These four values were approximated by simple functions of the height of burst. In some cases, a constant function was used; in other cases, a rational fraction was used. Certain constraints were imposed on the rational fraction to insure satisfactory behavior of the approximation.

d. Since parameter functions  $p_{dij}(h)$  only approximated values  $\hat{p}_{dij}(h_k)$ ,  $k = 1$  to 4, it was desirable to readjust the amplitudes of the driver functionals  $F_d(t, x, y, z; p_{dij}(h))$  to obtain a closer fit to the Monte Carlo data. Since the amplitude was by choice one of the parameters--specifically,  $p_{d1j}$ , this readjustment involved simply reoptimizing the fit to the Monte Carlo data by adjustment of this one parameter,  $p_{d1j}$ . Once this adjustment was done for each of the four heights of burst, amplitude parameter function  $p_{d1j}(h)$  was refitted to these four improved values for  $\hat{p}_{d1j}(h_k)$ .

e. This completed the definition of all parameter functions  $p_{dij}(h)$  for a particular neutron energy band,  $j$ . Process b to d was repeated for each of the nine energy bands.

This strategy was implemented through the use of two specially developed computer codes, BIGFIT and HOBFIT. BIGFIT performs a global minimization (that is, simultaneously over all volume detectors and time bins) of an error function estimating the "badness of fit" of driver functionals  $F_d$  to the Monte Carlo data. HOBFIT approximates the burst height dependence of parameter values  $\hat{p}_{dij}(h_k)$  with either a constant function or a rational function. BIGFIT performs the minimization for specified parameters of the functional. In practice, the specified parameters were usually either the amplitude parameter only or all parameters of the functional.

The curve-fitting procedure is illustrated in figure 1. This procedure was performed for each source neutron energy band and each driver functional, or  $9 \times 13 = 117$  times, except where the driver was exactly zero for an energy band. (For example, no high-energy neutron reactions can occur for a low-energy source neutron.) First, starting with trial guesses for the parameter values, BIGFIT was run four times (once for each burst height) to fit the driver functional to the Monte Carlo data for that case. All parameters were adjusted to obtain the fit. The functional parameter values so determined were stored in temporary data file FITFILE. Second, HOBFIT obtained functions approximating the burst height dependence of the parameters stored on FITFILE, saving these functions on permanent data file HOBFILE A. Third, the parameter functions were evaluated at the four burst heights, and the resulting parameter values were used as BIGFIT was rerun four times (once for each burst height) to fit the driver functional to the Monte Carlo data, this time adjusting only the amplitude parameter of the functional. The four amplitude parameter values so obtained were stored in temporary data file AMPFIT. Fourth, HOBFIT obtained a function approximating the burst height dependence of the revised amplitude parameter values on AMPFIT, saving this function on permanent data file HOBFILE B. Thus, the final amplitude parameter fits are stored on HOBFILE B, and the other parameter fits are stored on HOBFILE A.





piecewise fit to the space or time dependence of the data. For a global fit, a penalty function is constructed that measures the suitably weighted error or the disagreement between the data and the curve fit. The curve fit is improved by reducing the magnitude of the penalty function by adjustment of the fit parameters. A best fit is obtained when the penalty function arrives at a (minimum) extremum. The penalty function is a function of the several parameters for the driver functional and, with suitable smoothness, is amenable to minimization by standard optimization algorithms.

To illustrate the curve-fitting procedure, a specific example of a driver functional is examined. Neglecting air density and mass-scaling effects for simplicity of presentation, the functional for ionization by high-energy neutron inelastic collisions in the atmosphere (that is, "air inelastic" gamma ray production) is

$$I(x,y,z,t) = p_1 A C D$$

where

$x,y,z$  = Cartesian coordinates of the observer measured from the coordinate center on the ground beneath the burst,

$t$  = retarded time at the point  $(x,y,z')$ ,

$z'$  =  $z - h$ ,

$h$  = burst height,

$p_1$  = amplitude parameter,

$A$  =  $1 - p_2 \exp(-zp_3)$ ,

$C$  =  $\exp(-tp_4)/(t^{p_5} + p_6)$ ,

$D$  =  $\exp(-rp_7)/(r^2 + p_8)$ ,

$r$  =  $[x^2 + y^2 + (z')^2]^{1/2}$ .

This particular driver functional is relatively simple and incorporates range attenuation factor  $D$ , time dependence factor  $C$ , and ground depletion factor  $A$ . These factors are typical of other driver functionals, as well, although other functionals may also include time-dependent or range-dependent ground depletion (or enhancement) factors. Different time-dependence factors are used also.

In this functional, eight parameters are used so that the penalty function is a function of eight variables. The penalty function is defined as function P of parameter vector  $p_k$ ,  $k = 1$  to 8:

$$P(p_k) \equiv \sum_{i,j} \left\{ [f_{ij} - f(x_i, y_i, z_i, t_j; p_k)]^2 \frac{w_{ij}}{v_{ij}} \right\},$$

where the summation is performed over all  $i$  and  $j$  and where

- $i$  = a volume detector index running from 1 to 63,
- $j$  = a time bin index running from 1 to 19,
- $f_{ij}$  = the driver Monte Carlo score in the  $i$ th detector and  $j$ th time bin,
- $f(x_i, y_i, z_i, t_j; p_k)$  = the integral, over the  $i$ th detector and  $j$ th time bin, of driver functional  $F(x_i, y_i, z_i, t_j; p_k)$  (d subscript omitted from F) evaluated for parameter vector  $p_k$ ,
- $w_{ij}$  = a nonnegative weight factor defined as  $w_{ij} f_{ij}^2 / \hat{f}_{ij}^2$ ,
- $\hat{f}_{ij}$  = the total ionization score in the  $i$ th detector and the  $j$ th time bin due to all drivers (for ionization, these are high and low energy n- $\gamma$  reactions in air and in ground and neutron direct ionization),
- $w_{ij}$  = a user-defined nonnegative weight function emphasizing the importance of certain spatial regions (typically, about 10.0 near the ground and decreasing to about 0.25 to 1.0 at 1 km above the ground),
- $v_{ij}$  = the variance of score  $f_{ij}$ .

Score  $f_{ij}$  would be reproduced exactly by integral  $f(x_i, y_i, z_i, t_j; p_k)$  if driver functional F were an exact fit to the driver and if the variance associated with Monte Carlo score  $f_{ij}$  were zero. In this instance,  $P(p_k)$  would be zero. In actuality, functional F is not an exact fit, and variance V is proportional to the square of a fractional deviation averaging about 20 percent for the data given.

It is apparent that minimization of  $P(p_k)$  yields a weighted least-squares fit. The use of the inverse of variance  $V_{ij}$  increases the weight of low-variance Monte Carlo data, which is expected to be more accurate than high-variance data in inverse proportion to the variance. The use of ratio  $f_{ij}^2/\hat{f}_{ij}^2$  causes the relative importance of this driver to be considered in comparison with all the other contributing drivers. If the ratio is small, the weight is diminished accordingly; if the ratio is near unity (that is, no other driver is contributing significantly), the weight is maximized. User-defined factor  $w_i$  is used to force the best fit to be obtained near the ground (large  $w_i$ ) and a moderately good fit far from the ground (small  $w_i$ ). A very good fit near the ground is desired because most EMP targets (that is, electronic systems) are found on or near the ground.

To evaluate the quadruple integral,

$$f(x_i, y_i, z_i, t_j, p_k) \equiv \iiint_{V_i} dx dy dz \int_{t_{j-1}}^{t_j} dt F(x_i, y_i, z_i, t_j, p_k) ,$$

over detector volume  $V_i$  and time bin  $(t_{j-1}, t_j)$ , a numerical integration must be done. This numerical integration must be done efficiently because integral  $f$  must be evaluated  $63 \times 19 = 1197$  times for each evaluation of penalty function  $P$ . Penalty function  $P$  must typically be evaluated several hundred times to locate a useful minimum and the associated best fit. Thus, the numerical integration may be required about  $10^5$  times to complete one of the necessary  $4 \times 13 \times 9 = 468$  runs of BIGFIT. This is about  $10^7$  integral evaluations for the entire fitting problem. Evaluation of functional  $F$  requires roughly  $10^{-3}$  s of computer central processor (CP) time, so that about  $10^4 N$  seconds of CP time are forecast if  $N$  evaluations of functional  $F$  are needed to obtain its numerical integral  $f$ . Clearly,  $N$  must be as near unity as possible to avoid prohibitive computer time requirements. Accordingly, a three-point Gauss-Legendre quadrature was used for the time integration, and a special, highly accurate two-point Gaussian quadrature (with adjustable weight function) was developed by this writer and used for the volume integration. Appendix A describes the two-point scheme. Several other techniques were used to reduce the overall CP time requirement to about 40 hr for the entire curve-fitting project.

With the penalty function thus defined for the driver functional, it is necessary to minimize the penalty function by adjustment of the parameter vector. A highly efficient minimization algorithm is desired, in the sense of using the fewest possible evaluations of the penalty function. A number of different minimization algorithms were tested.

The most efficient algorithm for this application was determined to be a modified conjugate gradient method. This writer adapted the well-known conjugate gradient method<sup>8</sup> to use finite differences to estimate the gradient matrix and to cycle indefinitely during a single descent procedure instead of repeating the descent procedure after cycling once for each element in the vector of independent variables. A very efficient algorithm with quadratic convergence also was developed to search for a minimum along a chosen direction, in connection with the descent procedure. Appendix B contains a listing of the FORTRAN version of these descent algorithms. It was found that minimization of the penalty function proceeded much more rapidly if amplitude parameter  $p_1$  were optimized analytically during evaluation of penalty function  $P(p_k)$ . Optimum amplitude  $\alpha$  (to minimize  $P(p_k)$  with respect to the amplitude parameter) can easily be shown to be trial amplitude  $\alpha_t$  multiplied by the factor

$$K = \frac{\sum_{i,j} f_{ij} f(x_i, y_i, z_i, t_j; p_k) g_{ij}}{\sum_{i,j} [f(x_i, y_i, z_i, t_j; p_k)]^2 g_{ij}},$$

where, as previously explained,

$f_{ij}$  = the data value for volume detector  $i$  and time bin  $j$ ,

$f()$  = the corresponding value of the fit using a nonzero trial value (completely arbitrary) for  $p_1$ ,

$g_{ij}$  = corresponding complete weight function  $W_{ij}/V_{ij}$  used in penalty function  $P(p_k)$ .

When  $p_1$  is chosen in this way to be  $\alpha = K\alpha_t$  and when the minimization of  $P(p_k)$  is done for the other  $p_k$  exclusive of  $p_1$ , the minimization process is greatly accelerated.

Minimizing the penalty function (that is, obtaining the best fit) can be interpreted geometrically as finding the bottom of a hypersurface whose dimensionality is the number of functional parameters. An initial guess for the  $p_k$  provides a starting point for the descent. Taking an initial guess that is close to the true bottom reduces the descent effort and helps keep the descent path out of undesirable local minima that are far from the true bottom (that is, the least minimum). Although the computer calculation was performed in double precision, it

<sup>8</sup>R. Fletcher and C. M. Reeves, *Function Minimization by Conjugate Gradients*, *Computer Journal*, 7 (1964), 149-154.

was learned that a minimum in the hypersurface takes on a rough, granular texture in its shallowest portions due to roundoff errors in the calculation. This undesirable texture impedes the descent to the desired minimum. In general, the speed of descent is slowed by complexity or exceptional shallowness of the hypersurface. Greater complexity is typically caused by more parameters having higher polynomial degree than quadratic (in a Taylor expansion of the penalty function) so that the descent requires more changes in direction. Shallowness increases in rough proportion to the number of scattered data being fitted with the functional. For example, if the number of data is increased tenfold, but the data scatter (due to finite variance) is not reduced, the hypersurface becomes roughly 10 times shallower. It then becomes harder to find the precise bottom of the shallower surface. In this work, the penalty function hypersurface is both complex and shallow, and the success of the fitting process depended critically on the efficiency and the robustness of the minimization procedures.

The initial guesses for the various sets of parameters  $p_k$  were usually taken from the optimal values of  $p_k$  for adjacent source neutron energy bands or burst heights. After the optimum values for  $p_k$  were obtained for a particular descent, the importance of each parameter was tested. If elimination of a parameter caused a sizeable increase in the penalty function, that parameter was deemed important. If a negligible increase was observed, that parameter was deemed unimportant and was removed from the functional. The functionals for several drivers were considerably simplified in this way.

An example of the effect of minimizing the penalty function is shown for one volume detector in table 2. The energy deposition (or ionization) due to thermal neutron capture in the ground is given for volume detector 33, source neutron energy band 9 (8.19 to 15.0 MeV), and 200-m burst height. Detector 33 is 600 m to 900 m above the ground at 1200- to 1500-m ground range from the burst. Table 2 gives these parameters:

the time bin boundaries,

$f_{ij}$ , the Monte Carlo score in the detector,

$f$ , the optimal global fit score in the detector,

$f_T$ , the trial global fit score in the detector,

$d_{ij}$ , the percentage of fractional deviation (due to the variance) of the Monte Carlo score for this driver,

$\hat{d}_{ij}$ , the percentage of fractional deviation (due to the variance) of the Monte Carlo score for the sum of all drivers,

$r$ , the percentage fraction of the total Monte Carlo score,  $\hat{f}_{ij}$ , due to this driver,  $f_{ij}$  ( $r = 100 f_{ij}/\hat{f}_{ij}$ ),

$e$ , the percentage of difference between the Monte Carlo score,  $f_{ij}$ , and the optimal fit score,  $f$ ,

$\hat{e}$ , the percentage of "error" in the total score contributed by optimal fit score  $f$ ,

$e_T$ , the percentage of difference between Monte Carlo score  $f_{ij}$  and trial fit score  $f_T$ ,

$\hat{e}_T$ , the same as  $\hat{e}$ , but evaluated for the trial fit score  $f_T$ .

The goal of the fitting process is to make  $e$  as small as possible in each time bin. When  $r$  is larger, a better fit is needed to make  $e$  small and thereby make  $\hat{e}$  small. Generally,  $e$  is desired to be roughly equal to or smaller than  $d_{ij}$  for each time bin. Since fractional deviation  $d_{ij}$  (due to the variance) is an estimate of the Monte Carlo error, difference  $e$  between the fit and the Monte Carlo score should be about equal to  $d_{ij}$ . Thus, when  $d_{ij}$  is large,  $e$  may be large; when  $d_{ij}$  is small,  $e$  should be small. In table 2, time bins 11 through 13 have  $d_{ij}$  averaging 20 to 25 percent and  $e$  averaging about 10 percent; time bins 15 through 18 have  $d_{ij}$  averaging 40 to 50 percent and  $e$  averaging about 40 percent. The values for  $e$  and  $\hat{e}$  appear to fluctuate approximately randomly about zero in time bins 8 through 19, as would be expected of a good fit to the data. The largest values for  $e_T$  and  $\hat{e}$  have been reduced by the fitting process to smaller values for  $e$  and  $\hat{e}$ .

TABLE 2. EFFECT OF MINIMIZING PENALTY FUNCTION FOR IONIZATION RATE, VOLUME  
DETECTOR 33, NEUTRON ENERGY BAND 9 (8.19 TO 15.0 MeV), 200-m  
BURST HEIGHT

Time bin	Start of time bin (s)	$f_{ij}$	$f$	$f_T$	$d_{ij}$	$\hat{d}_{ij}$	$r$	$e$	$\hat{e}$	$e_T$	$\hat{e}_T$
1	0.0	0.0	0.8902D-12	0.9283D-12	99.9	9.3	0.0	100.0	0.0	100.0	0.0
2	0.1000D-06	0.7037D-08	0.3749D-11	0.3910D-11	99.9	10.8	0.1	-99.9	-0.1	-99.9	-0.1
3	0.2150D-06	0.0	0.8655D-11	0.9026D-11	99.9	11.4	0.0	100.0	0.0	100.0	0.0
4	0.4640D-06	0.0	0.1905D-10	0.1987D-10	99.9	10.9	0.0	100.0	0.0	100.0	0.0
5	0.1000D-05	0.0	0.4053D-10	0.4228D-10	99.9	9.9	0.0	100.0	0.0	100.0	0.0
6	0.2150D-05	0.0	0.8309D-10	0.8671D-10	99.9	10.6	0.0	100.0	0.0	100.0	0.0
7	0.4640D-05	0.0	0.1588D-09	0.1659D-09	99.9	9.4	0.0	100.0	0.0	100.0	0.0
8	0.1000D-04	0.3858D-09	0.2659D-09	0.2780D-09	78.2	11.7	0.2	-31.1	-0.1	-27.9	-0.1
9	0.2150D-04	0.3121D-09	0.3653D-09	0.3814D-09	76.7	7.1	0.3	14.6	0.0	18.2	0.1
10	0.4640D-04	0.2202D-09	0.4027D-09	0.4155D-09	64.9	9.0	1.0	45.3	0.4	47.0	0.5
11	0.1000D-03	0.3823D-09	0.3606D-09	0.3580D-09	17.6	9.6	7.0	-5.7	-0.4	-6.4	-0.4
12	0.2150D-03	0.2123D-09	0.2503D-09	0.2255D-09	20.9	9.2	26.8	15.2	4.1	5.9	1.6
13	0.4640D-03	0.1282D-09	0.1143D-09	0.8529D-10	29.3	23.7	80.6	-10.8	-8.7	-33.5	-27.0
14	0.1000D-02	0.3546D-10	0.3013D-10	0.1921D-10	69.2	58.4	83.7	-15.0	-12.6	-45.8	-38.3
15	0.2150D-02	0.6082D-11	0.8749D-11	0.6371D-11	43.6	36.6	63.4	30.5	19.3	4.5	2.9
16	0.4640D-02	0.2689D-11	0.3813D-11	0.2867D-11	50.3	28.7	13.9	29.5	4.1	6.2	0.9
17	0.1000D-01	0.3794D-11	0.1688D-11	0.1283D-11	39.2	25.5	27.7	-55.5	-15.4	-66.2	-18.3
18	0.2150D-01	0.1349D-11	0.7428D-12	0.5717D-12	52.4	15.5	15.8	-44.9	-7.1	-57.6	-9.1
19	0.4640D-01	0.3319D-12	0.3262D-12	0.2542D-12	35.0	17.5	7.6	-1.7	-0.1	-23.4	-1.8

Notes:

$f_{ij}$  = the Monte Carlo score in the detector.

$f$  = the optimal global fit score in the detector.

$f_T$  = the trial global fit score in the detector.

$d_{ij}$  = the percentage of fractional deviation (due to the variance)  
of the Monte Carlo score for these drivers.

$\hat{d}_{ij}$  = the percentage of fractional deviation (due to the variance)  
of the Monte Carlo score for the sum of all drivers.

$r = 100 f_{ij} / \hat{d}_{ij}$ .

$e$  = the percentage of difference between  $f_{ij}$  and  $f$ .

$\hat{e} = re/100$ .

$e_T$  = the percentage of difference between  $f_{ij}$  and  $f_T$ .

$\hat{e}_T = re_T/100$ .

## 6. BURST HEIGHT DEPENDENCE OF FIT PARAMETERS

Having obtained parameter values at four burst heights, we desired to develop smooth functions of burst height to approximate the parameter values. Some scatter was evident in the burst height dependence. The functions chosen should avoid reproducing the scatter, but capture the important trend of the data. Two burst height functions were selected: (1) the constant function, independent of burst height, and (2) the rational function

$$g(h) = \frac{C_1 + C_2h + C_3h^2}{1 + C_4h^2} ,$$

where  $h$  is the burst height and  $C_i$  are fit coefficients. By inspection of the parameter values at the four burst heights, the author determined which of the two burst height functions was appropriate for a parameter. Many parameters were clearly independent of burst height. Other parameters displayed such severe scatter that it was necessary to use merely an average value for all burst heights. On the other hand, many parameters showed well-defined trends and were fitted with rational functions.

Fitting the four values of a parameter with a rational function was not a trivial problem. In its application to real EMP prediction problems, the rational function would be evaluated at other burst heights. Therefore, the behavior of the rational function must be carefully controlled for all possible burst heights. For example, simply fitting the four parameter values with rational function  $g(h)$  would reproduce the data exactly, but might introduce poles, crossovers, and similar erratic behavior at other burst heights. To avoid this possibility, several stratagems were adopted. First, the fit was to be done by use of Courant's well-known penalty function method for optimization with nonlinear constraints, and the nonlinear constraints would be defined so as to inhibit the erratic behavior. Second, the rational function would be made to fit not the four data, but the piecewise linear function  $\hat{p}$  interpolating the four data.

The penalty function used was

$$Q(C_1; r) = \sum_j [g(h_j) - \hat{p}(h_j)]^2 + r(N_1 + N_2 + N_3) .$$



The  $h_j$  are about 40 burst heights on the interval from 1 to 300 m.  $N_1$ ,  $N_2$ , and  $N_3$  are positive semidefinite functions that are zero when a corresponding constraint is satisfied. In the optimization process,  $Q$  is minimized for successively larger values of  $r$  by using as each starting point the previous optimum values for  $C_i$ . As  $r$  is increased to infinity,  $Q$  becomes optimal for the constraints represented by  $N_1$ ,  $N_2$ , and  $N_3$ . The specific nonlinear constraints were these:

- a. For complex  $h$ , no poles of  $g(h)$  in the right half-plane of  $h$ ,

$$N_1 = 10^8 [\min(0, C_4)]^2 ,$$

- b. No crossover to negative values of  $g(h)$  for large  $h$ ,

$$N_2 = 10^8 [\min(0, C_3)]^2 / \hat{p}(200 \text{ m}) ,$$

- c. No negative values for  $g(h)$  for small  $h$ ,

$$N_3 = [\min(0, C_1)]^2 / \hat{p}(200 \text{ m}) .$$

The minimization of  $Q$  was done for each value of  $r$  by adjusting the four  $C_i$ . The descent algorithms described in section 5 were used. For burst heights above 200 m, most driver parameters tend toward limiting values not much different from the value at the 200-m burst height. An exception is the amplitude parameter for a ground-induced source. This parameter should decay monotonically to zero as the burst height increases. For burst heights above 250 m, the three high-energy ground driver amplitudes are made to decay by a factor of two for each additional 100 m. Similarly, the three low-energy ground driver amplitudes are made to decay by a factor of 1.2 to 4, depending on the source neutron energy, for each additional 100-m increase in burst height over 250 m.

## 7. COMPARISON WITH LIQUID AIR EXPERIMENT

Sidhu et al<sup>9</sup> measured neutron and secondary gamma ray transport through a liquid air sphere for a 14-MeV neutron source. Their 129.3-cm sphere radius was equivalent to an atmospheric range of 850 m. They published (their fig. 7) for secondary gamma rays a value of about  $1.3 \times 10^{-10} \text{ cm}^2\text{-rad (tissue)/source neutron}$  for the  $4\pi r^2$  dose at 850-m equivalent range in air. The corresponding value for the NEMP code energy band 9 (8.19 to 15.0 MeV) high-energy air driver is  $1.5 \times 10^{-10} \text{ cm}^2\text{-rad (air)}$ . One rad in tissue and one rad in air differ by only about 1 percent, so these gamma doses differ by about 15 percent.

<sup>9</sup>G. S. Sidhu, W. E. Farley, L. F. Hansen, T. Komoto, B. Pohl, and C. Wong, *Transport of Neutron and Secondary Gamma Radiations Through a Liquid Air Sphere Surrounding a 14-MeV Neutron Source*, *Nuclear Science and Engineering*, 66 (June 1978), 428-433.

The NEMP neutron dose in air cannot be compared easily with the measured neutron tissue dose because neutron kerma\* factors are very energy dependent in the range from 1 to 14 MeV. The neutron energy spectrum at the 850-m observer for the NEMP driver is unavailable to allow a conversion from neutron air dose to neutron tissue dose.

Shown in figure 7 of Sidhu et al<sup>9</sup> are results of TARTNP computer code calculations of the gamma tissue dose. The TARTNP code is a discrete ordinates radiation transport code used at the Lawrence Livermore Laboratories. The results show the  $4\pi r^2$  dose to a 2800-m range. Differences between the NEMP driver and TARTNP results appear to be small (a few percent) from 850 to 2500 m. The NEMP code results are roughly 15 percent lower at the 500-m range.

#### 8. COMPARISON WITH EARLIER APPROXIMATION FOR IONIZATION BY 14-MeV NEUTRONS

Longley et al<sup>5</sup> developed approximations for EMP drivers for use in their LEMP 2 surface burst EMP environment prediction code. They used Longmire's analytic first-scatter theory and many-scatter diffusion theory to describe 14-MeV neutron direct ionization through elastic scattering and (n,p) reactions. Comparison of their 14-MeV neutron driver with the corresponding NEMP driver (energy band 9, direct neutron ionization) showed rough agreement and some differences. For dose in air, the NEMP results exhibited a 10-percent longer attenuation length at all ranges and a roughly 50-percent greater amplitude (factoring out the range dependence). Because detailed reaction cross sections were not used for this LEMP 2 driver (per C. L. Longmire, Mission Research Corp.), some disagreement is expected.

Since the LEMP 2 drivers are independent of the source neutron energy spectrum (except for 14-MeV neutrons), a comparison with the nine energy band NEMP drivers is a complicated undertaking beyond the scope of this report.

---

<sup>5</sup>H. J. Longley, C. L. Longmire, J. S. Malik, R. M. Hamilton, R. N. Marks, and K. S. Smith, Development and Testing of LEMP 2, A Surface Burst EMP Code (U), Mission Research Corp., Santa Barbara, CA, DNA 4097T (December 1976). (CONFIDENTIAL)

<sup>9</sup>G. S. Sidhu, W. E. Farley, L. F. Hansen, T. Komoto, B. Pohl, and C. Wong, Transport of Neutron and Secondary Gamma Radiations Through a Liquid Air Sphere Surrounding a 14-MeV Neutron Source, Nuclear Science and Engineering, 66 (June 1978), 428-433.

\*The total kinetic energy of directly ionizing particles ejected by the action of indirectly ionizing radiation per unit mass of specified material.

## 9. SELECTED RESULTS

Time histories of some NEMP neutron-induced EMP drivers are portrayed in figures 2 to 13. Radial Compton current, theta Compton current, and ionization rate are plotted. Results are shown for two observers 0 and 500 m above the ground for each of two burst heights of 1 and 200 m. The ground range from the burst to the observer is 1000 m. All results are for a source of one neutron in the energy band of 8.19 to 15.0 MeV. Although drivers for other neutron energy bands have different amplitudes, attenuation lengths, burst height dependence, air-ground interface effects, etc., these results are typical.

In the figures, each driver is represented by a broken line with identifying symbols. The "F" denotes the high-energy ground driver (ground inelastics); the "I" denotes the high-energy air driver (air inelastics); the "G" denotes the low-energy ground driver (ground captures); the "A" denotes the low-energy air driver (air captures); and the "N" denotes neutron direct ionization including charged particle ionization. The total for all drivers is represented by a solid line with identifying "T" symbols. Each curve is the magnitude, or absolute value, of the driver or total.

Several general observations can be made concerning burst height and observer height variations. High-energy ground drivers are significantly weaker for greater burst heights. Low-energy ground drivers decay more slowly with increasing burst height than do high-energy ground drivers because source neutrons penetrate to greater ranges while decaying to lower energies. Low- and high-energy air drivers and the neutron direct ionization driver all are roughly twice as strong for the 200-m burst height as for the 1-m burst height because roughly half of the source neutrons are absorbed by the ground for the lower burst height.

The drivers for theta Compton current are all stronger for observers closer to the ground surface because of the asymmetry presented by the air-ground interface. High-energy and low-energy air drivers for radial Compton current and ionization rate are relatively insensitive to observer height. The time dependence of the neutron direct ionization driver is different for the two observer heights considered. This driver is somewhat shorter in duration near the ground because many later-arriving multiply scattered neutrons tend to become trapped in the ground and do not contribute to the driver in the air. The low-energy

ground driver for ionization rate is somewhat stronger for the higher observer, more noticeably so for the 200-m burst height than for the 1-m burst height. They differ because the secondary gamma rays (produced by neutron capture in the ground) that drive the ionization rate at the observer must penetrate more soil to reach the shallower observer. The low-energy ground driver for radial Compton current is even more strongly decreased for observers near the ground because the net Compton current flow follows the direction of the gamma ray flux, which is predominantly up out of or down into the ground (perpendicular to the radial direction). Higher off the ground, more gamma rays with a nearly radial direction arrive from ground regions close to the burst.

All drivers contributing to the radial Compton current have the same sign (negative). The theta Compton current drivers may have different signs or even change sign. (By convention, positive is downward.) The theta Compton currents for high-energy ground and low-energy air drivers are positive and negative, respectively. The theta Compton current for the low-energy ground driver is generally negative at this range from the burst because of a secondary gamma ray "fountain" effect. This effect is due to many secondary gamma rays rising upward from the ground close to the burst and being turned down toward the ground after a few Compton collisions in the air. However, for observers close to the ground and close to the burst, enough upward-going secondary gamma rays are produced beneath the observer to reverse the theta Compton current from negative to positive for a period of time (fig. 9). The theta Compton current for high-energy air reactions was set identically to zero because it was about two orders of magnitude smaller than the corresponding radial Compton current and because the available Monte Carlo statistics for those data were so poor that a reliable fit was unlikely.

The time history of the high-energy ground drivers for theta Compton current and ionization rate deserves some explanation. It may consist of two pulses: one from the initial arrival of neutrons at the ground beneath the burst and the other from the arrival of neutrons at an area roughly midway between the burst and the observer. The secondary gamma rays produced in the ground have an attenuation length considerably greater than the mean free path of the neutrons. This greater length causes contributions from reactions (per unit ground surface area) beneath the burst to be more important than contributions from reactions very near the observer. However, gamma rays originating in the ground closer to the observer are less attenuated by the ground because of their higher angle of departure from the ground. This complicated

behavior was approximated by the two pulses mentioned. The approximation gives reasonable agreement with the Monte Carlo data, but too much importance should not be attached to the detailed structure of the time history approximation, especially since the data time bins were one-third of an order of magnitude wide. The second pulse of this two-pulse structure is not observed in the data (and the driver) for radial Compton current. Also, the second pulse is not observed in the data (and the driver) for ionization rate if the burst height is very near the surface (fig. 4 and 7) or if the observer is very high (fig. 13).

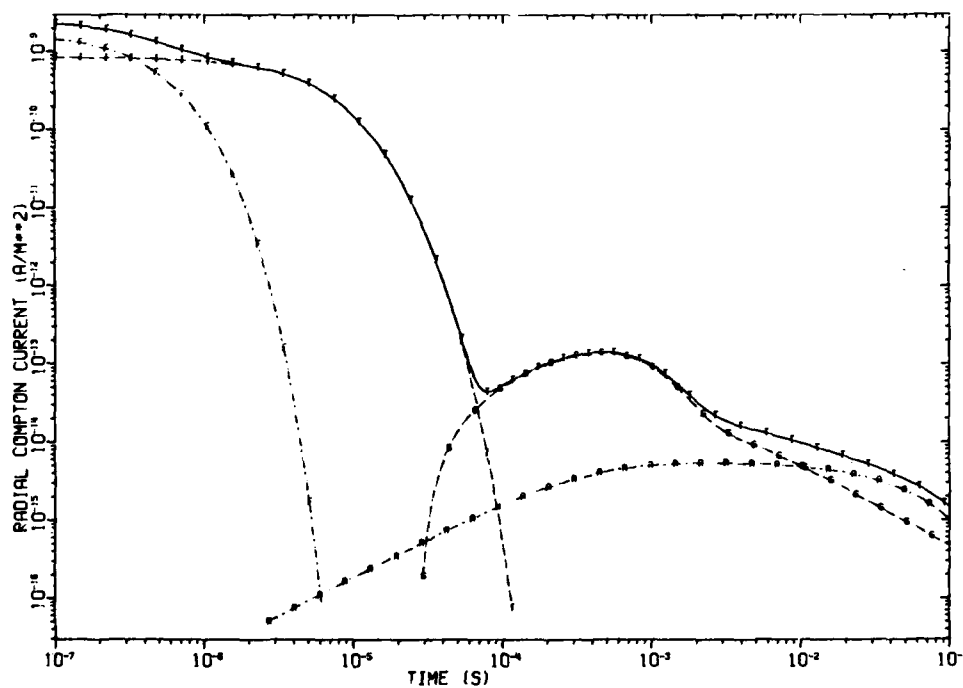


Figure 2. Radial Compton current for 1-m burst height, 0-m observer height, and 1000-m ground range.

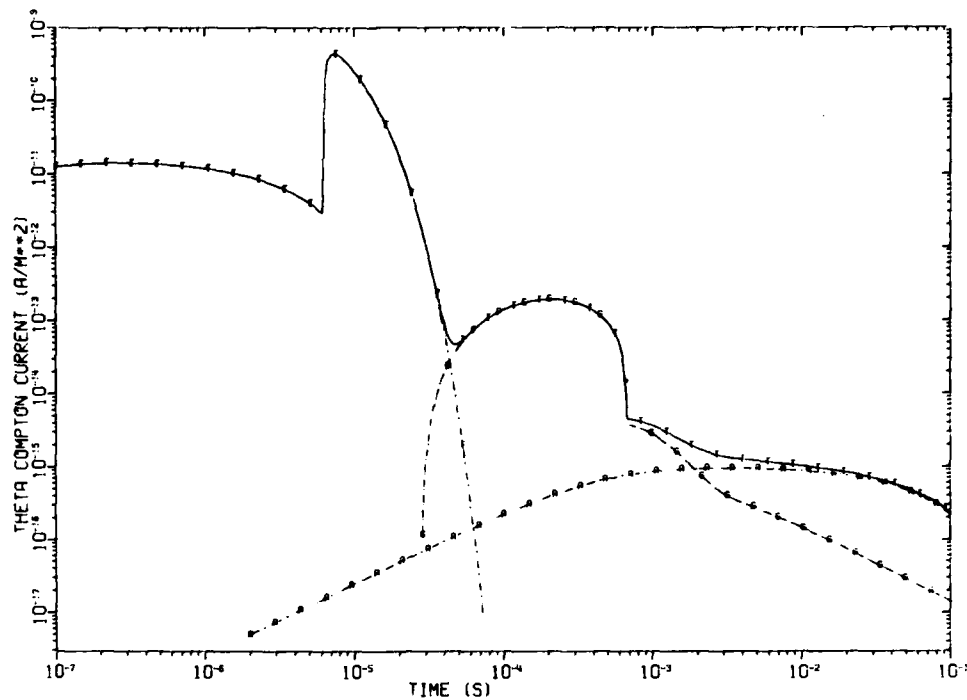


Figure 3. Theta Compton current for 1-m burst height, 0-m observer height, and 1000-m ground range.

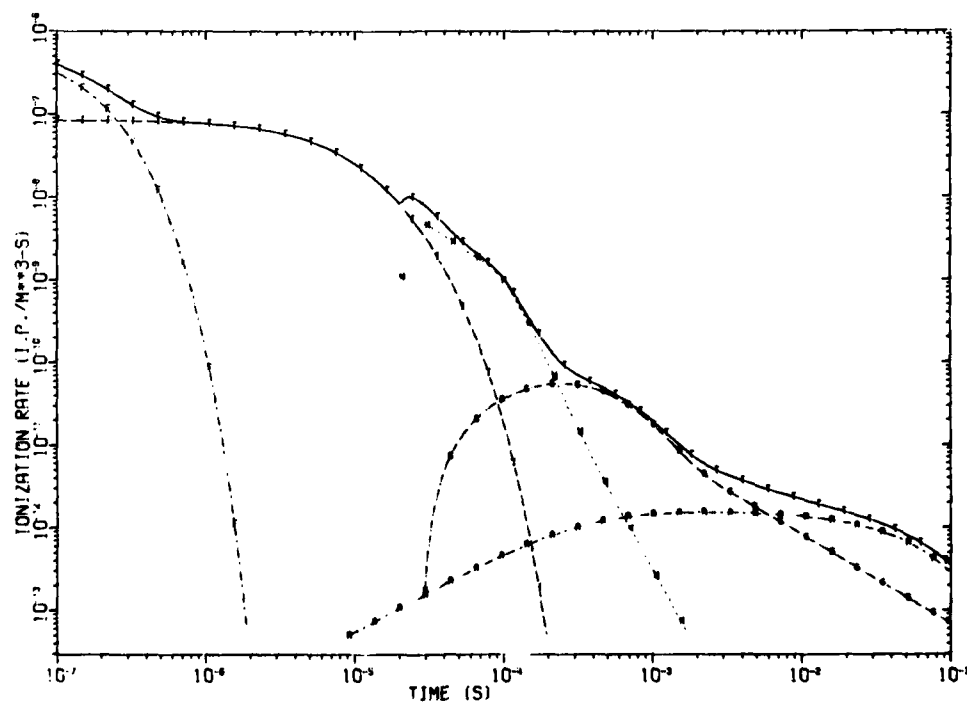


Figure 4. Ionization rate for 1-m burst height, 0-m observer height, and 1000-m ground range.

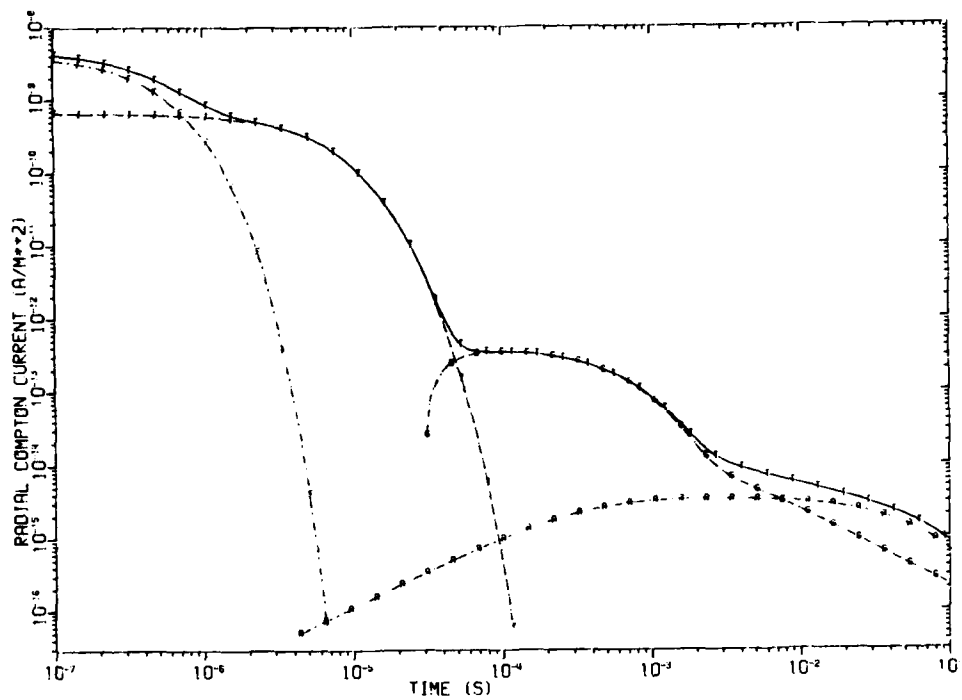


Figure 5. Radial Compton current for 1-m burst height, 500-m observer height, and 1000-m ground range.

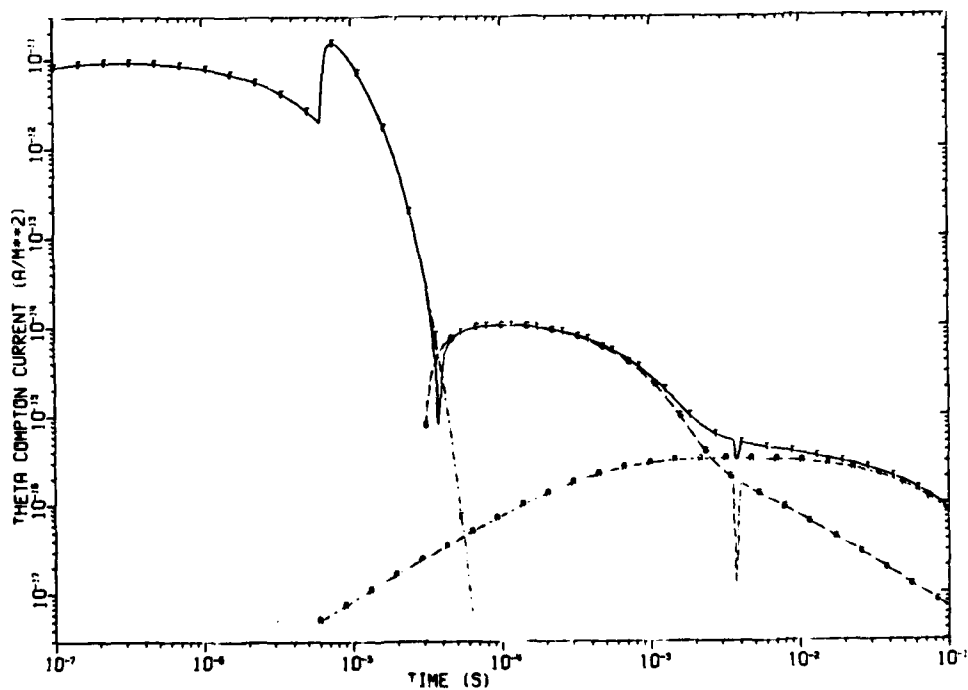


Figure 6. Theta Compton current for 1-m burst height, 500-m observer height, and 1000-m ground range.

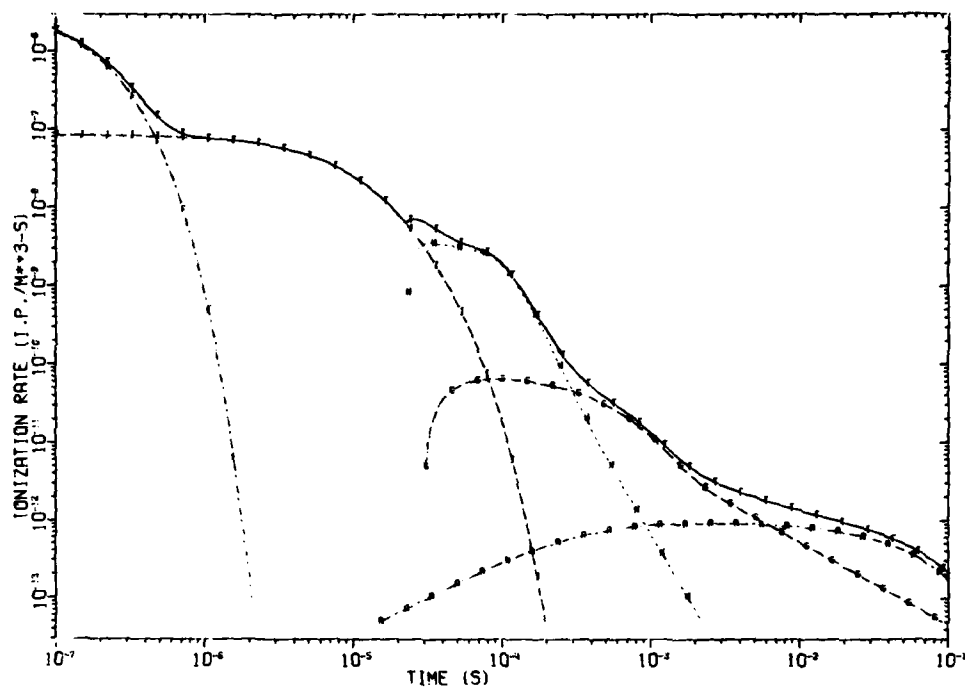


Figure 7. Ionization rate for 1-m burst height, 500-m observer height, and 1000-m ground range.

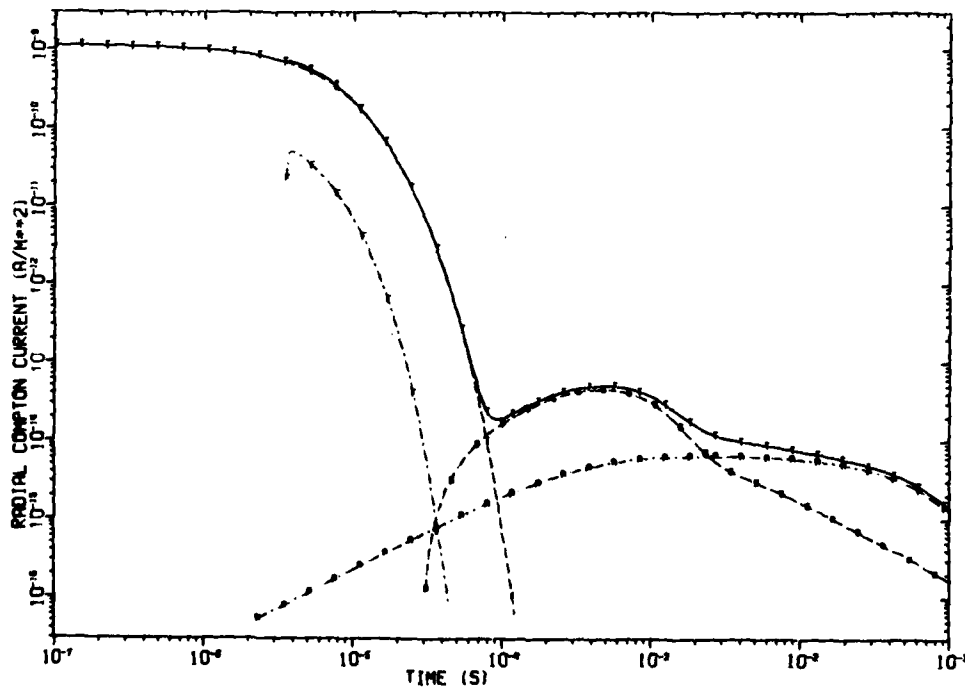


Figure 8. Radial Compton current for 200-m burst height, 0-m observer height, and 1000-m ground range.



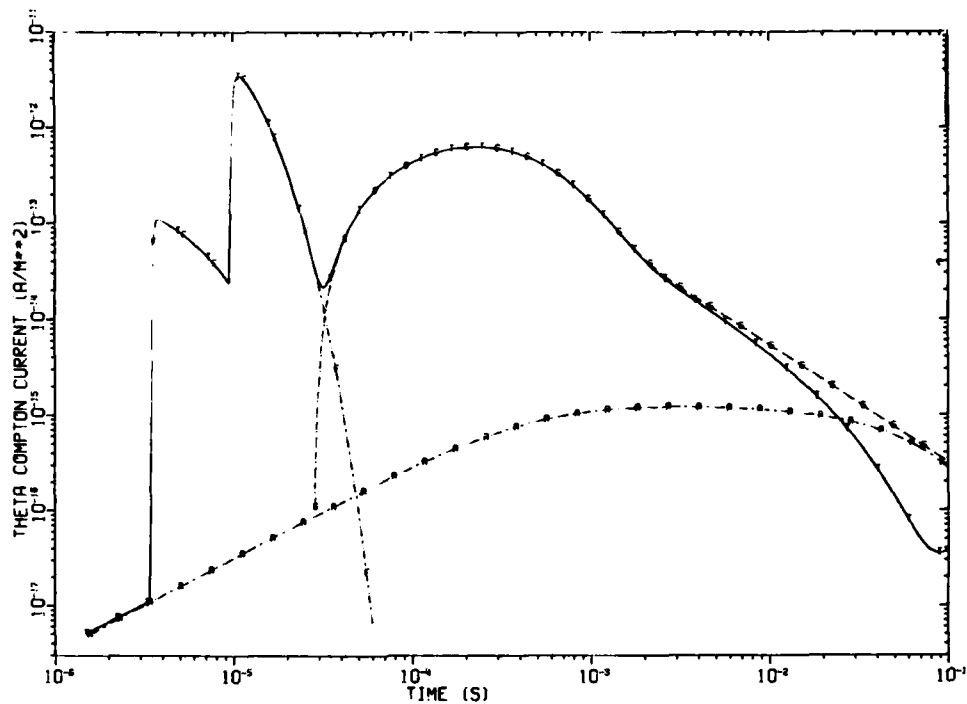


Figure 9. Theta Compton current for 200-m burst height, 0-m observer height, and 1000-m ground range.

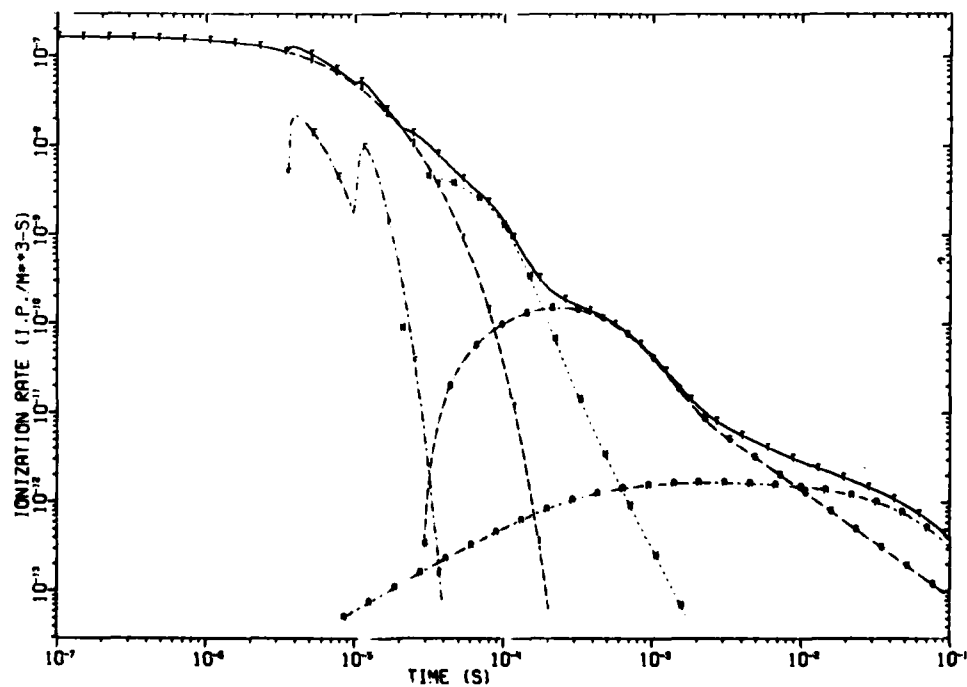


Figure 10. Ionization rate for 200-m burst height, 0-m observer height, and 1000-m ground range.

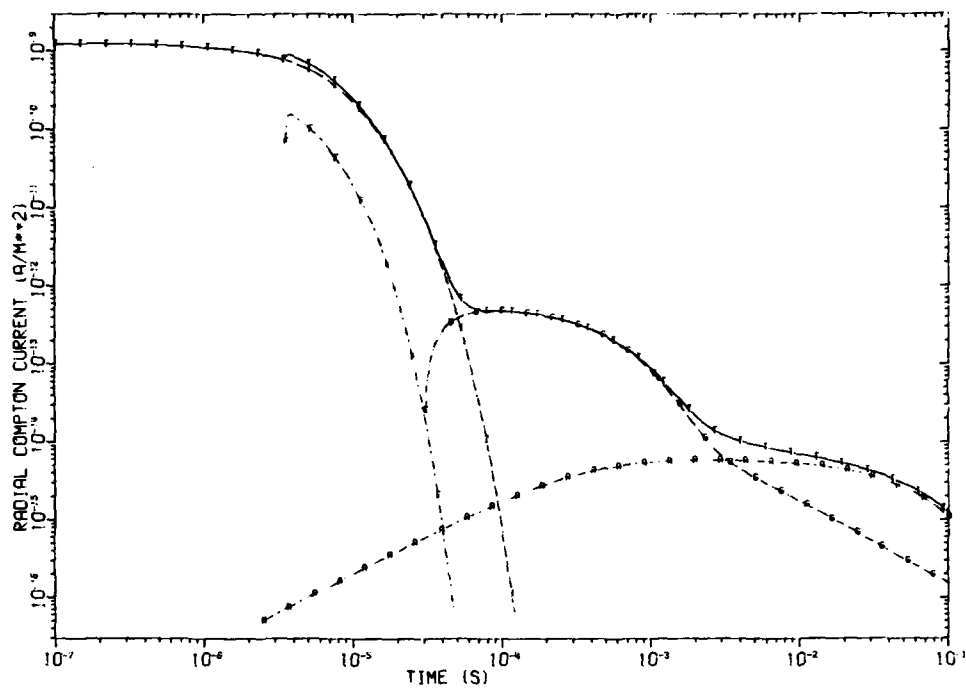


Figure 11. Radial Compton current for 200-m burst height, 500-m observer height, and 1000-m ground range.

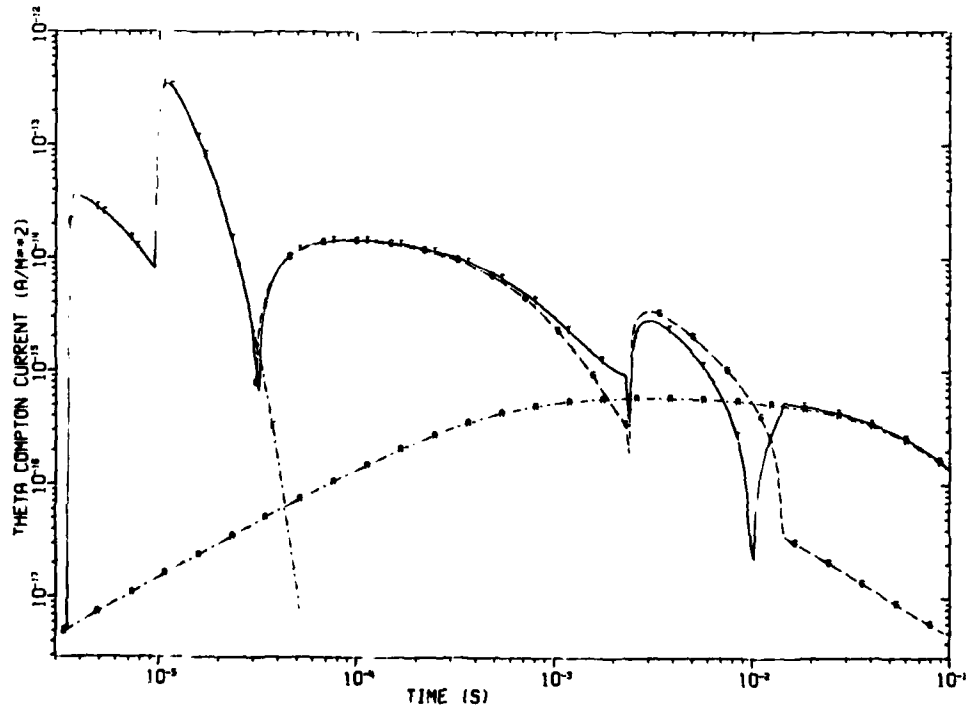


Figure 12. Theta Compton current for 200-m burst height, 500-m observer height, and 1000-m ground range.

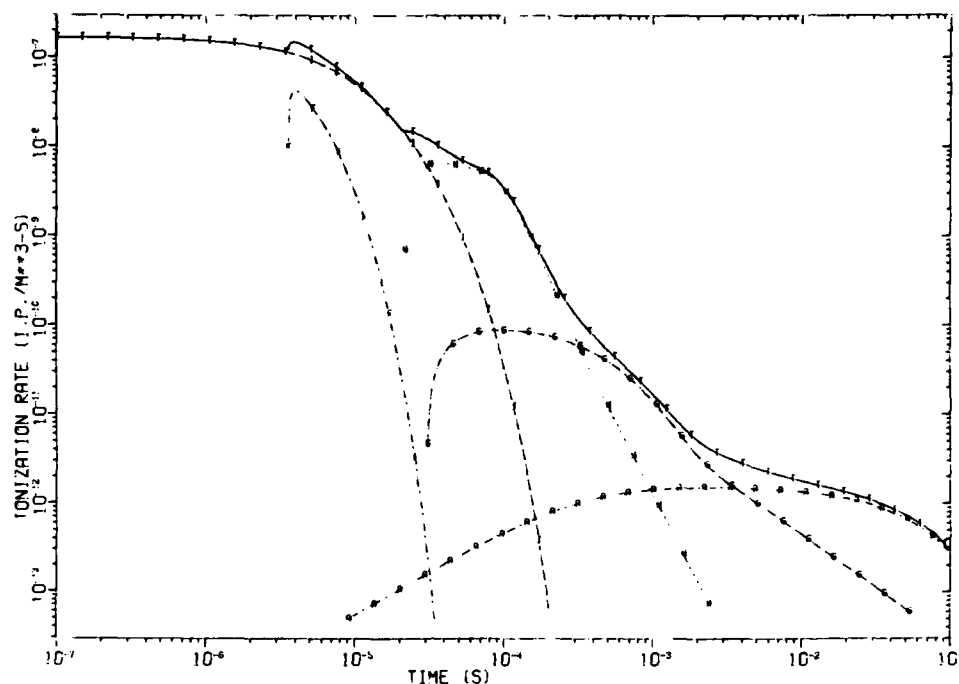


Figure 13. Ionization rate for 200-m burst height, 500-m observer height, and 1000-m ground range.

#### 10. CONCLUSIONS

The NEMP neutron-induced EMP driver package represents the state of the art for predicting EMP drivers from near-surface bursts, allowing flexible representation of any weapon's neutron energy spectrum and choice of any burst height in the near-surface regime. The package consists of separate space- and time-dependent drivers for radial and theta Compton current and ionization rate, for high- and low-energy reactions in the air and the ground, for nine source neutron energy bands, for any near-surface burst height.

This report has described the development of this EMP driver package for neutron-induced sources, for use in the NEMP code for EMP environment prediction for near-surface nuclear bursts. The development was based on the concept of obtaining a global fit of certain well-chosen functionals to Monte Carlo transport data over the entire set of volume detectors and time bins. The global fit obtained in this manner offered several advantages over fitting with polynomials, including the effective elimination of Monte Carlo "noise" and the possibility of reduction of error below the level of Monte Carlo statistical error. The fit also involved far fewer degrees of freedom. The global fit was obtained by minimization of a penalty function representing the badness

of fit. Because of the large amount of computer time involved, highly efficient minimization algorithms were employed. The difficulty of the minimization depended, among other things, on the variance of the Monte Carlo data, which averaged about 20 to 30 percent. The burst height dependence of the fit parameters was explicitly obtained for burst heights from 1 to 250 m. Extrapolation methods were devised for burst heights greater than 250 m.

Comparison of ionization from gamma rays induced by a 14-MeV neutron source with experimental measurements gave good agreement. Comparison with the LEMP 2 direct neutron ionization driver for 14-MeV neutrons revealed significant differences. Typical results were discussed for two burst heights and two observer heights, for the 8.19- to 15.0-MeV source neutron energy band drivers.

#### LITERATURE CITED

- (1) William T. Wyatt, Jr., A Near-Surface Burst EMP Driver Package for Prompt Gamma-Induced Sources, Harry Diamond Laboratories HDL-TR-1931 (September 1980).
- (2) H. J. Longley, C. L. Longmire, and K. S. Smith, Development of NEMP (U), Mission Research Corp., Santa Barbara, CA, HDL-CR-75-001-1 (April 1975). (SECRET--RESTRICTED DATA)
- (3) H. J. Longley and K. S. Smith, Developments in NEMP for 1977 (U), Mission Research Corp., Santa Barbara, CA, HDL-CR-77-0022-1 (January 1978). (SECRET--RESTRICTED DATA)
- (4) H. J. Longley and C. L. Longmire, Development and Testing of LEMP 1, Los Alamos Scientific Laboratory, NM, LA-4346 (April 1970).
- (5) H. J. Longley, C. L. Longmire, J. S. Malik, R. M. Hamilton, R. N. Marks, and K. S. Smith, Development and Testing of LEMP 2, A Surface Burst EMP Code (U), Mission Research Corp., Santa Barbara, CA, DNA 4097T (December 1976). (CONFIDENTIAL)
- (6) D. A. Sargis, E. R. Parkinson, J. N. Wood, R. E. Dietz, and C. A. Stevens, Late-Time Sources for Close-In EMP, Science Applications, Inc., La Jolla, CA, DNA 3064F (August 1972).
- (7) H. S. Schechter and M. O. Cohen, Energy Deposition Rates and Compton Electron Currents from Low-Altitude Bursts as a Function of Source Energy, Mathematical Applications Group, Inc., Elmsford, NY, HDL-CR-77-020-1 (November 1977)
- (8) R. Fletcher and C. M. Reeves, Function Minimization by Conjugate Gradients, Computer Journal, 7 (1964), 149-154.
- (9) G. S. Sidhu, W. E. Farley, L. F. Hansen, T. Komoto, B. Pohl, and C. Wong, Transport of Neutron and Secondary Gamma Radiations Through a Liquid Air Sphere Surrounding a 14-MeV Neutron Source, Nuclear Science and Engineering, 66 (June 1978), 428-433.

#### APPENDIX A.--A TWO-POINT QUADRATURE SCHEME

Integrating a driver functional over the entire volume of a volume detector can be very time-consuming if unsophisticated quadrature methods are used. The volume detector concerned is a square toroid, that is, a toroid with a square cross section in coordinates  $(x, z, \phi)$ . The toroid is bounded by  $X_1, X_2, Z_1$ , and  $Z_2$ , where  $x$  is the ground range from the coordinate center and  $z$  is the height above the ground. The driver has azimuthal symmetry around the center of the toroid ( $x = 0$ ) so that an integration in independent variable  $\phi$  is trivial. Thus, an integral over detector volume

$$I = \int_{X_1}^{X_2} \int_{Z_1}^{Z_2} \int_0^{2\pi} f(x, z) (x^2 + z^2)^{1/2} dx dz d\phi$$

becomes

$$I = 2\pi \int_{X_1}^{X_2} \int_{Z_1}^{Z_2} f(x, z) (x^2 + z^2)^{1/2} dx dz .$$

If  $f(x, z)$  describes a driver functional, the salient spatial gradients of  $f(x, z)$  are (1) in the vertical ( $z > 0$ ) direction due to proximity of the ground and (2) in the radial direction from the burst due to geometric and atmospheric attenuation. A particularly accurate Gaussian quadrature rule would use the geometric and atmospheric attenuation as a weight function.

Our goal is a Gaussian quadrature rule for the integral

$$J = \int_{X_1}^{X_2} \int_{Z_1}^{Z_2} v(x, z) w(x, z; \alpha) dx dz ,$$

where  $v$  is a function of  $x$  and  $y$  and  $w$  is a weight function defined by

$$w(x, z; \alpha) = \exp(-\alpha r) / (1 + r^2) ,$$

$$r = [x^2 + (z - h)^2]^{1/2} .$$

The burst height is  $h$ . The advantage of this weight function rests on the fact that it represents the actual spatial dependence (for a suitable choice of  $\alpha$ ) better than a low-order power series would. Parameter  $\alpha$  is essentially the atmospheric attenuation coefficient (the reciprocal of the attenuation length) and is available for use during

## APPENDIX A

the calculation of a driver integral. Thus, we may exploit our knowledge of  $\alpha$  to construct the quadrature based on weight function  $w(x,z;\alpha)$ . In computer program BIGFIT, we actually first construct a family of quadrature rules for a range of values  $\alpha_i$ . Then when a driver integral is being calculated, the  $\alpha_i$  nearest to  $\alpha$  is determined, and its corresponding quadrature rule is used. In this way, the construction of the quadrature rules is kept out of the inner program loops.

For the J integral quadrature rule, we seek quadrature points  $(x_1, z_1)$  and  $(x_2, z_2)$  with weight coefficients  $w_1$  and  $w_2$ , respectively. We require exact integration of Taylor series terms for  $x^0$  (and  $z^0$ ),  $x^1, z^1, z^2$ , and  $z^3$ . This requirement yields the following conditions on  $x_1, z_1, z_2, w_1$ , and  $w_2$ :

$$\begin{aligned} w_1 + w_2 &= M_{00} \quad , \\ w_1 x_1 + w_2 x_2 &= M_{10} \quad , \\ w_1 z_1 + w_2 z_2 &= M_{01} \quad , \\ w_1 z_1^2 + w_2 z_2^2 &= M_{02} \quad , \\ w_1 z_1^3 + w_2 z_2^3 &= M_{03} \quad , \end{aligned}$$

where

$$M_{ij} = \int_{x_1}^{x_2} \int_{z_1}^{z_2} x^i z^j w(x,z;\alpha) dx dz \quad .$$

This quadrature is separable in  $x$  and  $z$  and easy to obtain. Obviously,

$$x_1 = M_{10}/M_{00}.$$

Define the polynomial

$$P = (z - z_1)(z - z_2) = 0 \quad ,$$

or

$$P = z^2 - Az + B = 0 \quad .$$

# APPENDIX A

Multiply the preceding equations by A and B and add:

$$w_1 B + w_2 B = BM_{00}$$

$$w_1(Az_1) + w_2(Az_2) = AM_{01}$$

$$w_1(z_1^2) + w_2(z_2^2) = M_{02}$$

---


$$w_1(P) + w_2(P) = AM_{01} + BM_{00} + M_{02}$$

$$w_1 z_1(B) + w_2 z_2(B) = BM_{01}$$

$$w_1 z_1(Az_1) + w_2 z_2(Az_2) = AM_{02}$$

$$w_1 z_1(z_1^2) + w_2 z_2(z_2^2) = M_{03}$$

---


$$w_1 z_1(P) + w_2 z_2(P) = AM_{02} + BM_{01} + M_{03} \quad .$$

Since  $P = 0$ , we have

$$AM_{01} + BM_{00} + M_{02} = 0 \quad ,$$

$$AM_{02} + BM_{01} + M_{03} = 0 \quad ,$$

or solving for A and B,

$$A = (M_{03}M_{00} - M_{02}M_{01})/C \quad ,$$

$$B = (M_{02}^2 - M_{01}M_{03})/C \quad ,$$

where

$$C = M_{01}^2 - M_{00}M_{02} \quad .$$

Therefore,

$$z_1 = [-A - (A^2 - 4B)^{1/2}]/2 \quad ,$$

$$z_2 = [-A + (A^2 - 4B)^{1/2}]/2 \quad .$$



## APPENDIX A

Then

$$w_1 + w_2 = M_{00} ,$$

$$w_1 z_1 + w_2 z_2 = M_{01} ,$$

or

$$w_1 = (M_{01} - M_{00} z_2) / (z_1 - z_2) ,$$

$$w_2 = M_{00} - w_1 .$$

Suppose we seek to integrate

$$K = \int_{x_1}^{x_2} \int_{z_1}^{z_2} \mu(x, z) dx dz ,$$

where  $\mu(x, z)$  has dominant spatial variation  $w(x, z; \alpha)$ . We rewrite  $K$  as

$$K = \iint \left[ \frac{\mu(x, z)}{w(x, z; \alpha)} \right] w(x, z; \alpha) dx dz$$

and apply the quadrature rule developed to get

$$k = w_1 \left[ \frac{\mu(x_1, z_1)}{w(x_1, z_1; \alpha)} \right] + w_2 \left[ \frac{\mu(x_1, z_2)}{w(x_1, z_2; \alpha)} \right] .$$

It is best to combine  $w(x_1, z_1; \alpha)$  with  $w_1$  and  $w(x_1, z_2; \alpha)$  with  $w_2$  to obtain the modified rule

$$K = \hat{w}_1 \mu(x_1, z_1) + \hat{w}_2 \mu(x_1, z_2) ,$$

where

$$\hat{w}_1 = w_1 / w(x_1, z_1; \alpha) ,$$

$$\hat{w}_2 = w_2 / w(x_1, z_2; \alpha) .$$

Thus, a unique quadrature rule ( $x_1, z_1, z_2, \hat{w}_1$ , and  $\hat{w}_2$ ) was obtained for each combination of volume detector and  $\alpha_1$  before commencing the descent algorithm to fit a driver functional to Monte Carlo data. Then during the descent, the numerical integration of  $K$ -like integrals proceeded extremely rapidly.

## APPENDIX B.--DESCENT ALGORITHMS USED

This appendix lists the FORTRAN version of the descent algorithms used to search for a minimum of a function.

# APPENDIX B

```

SUBROUTINE TALCG(FN,X,TOL,B,G,XOLD,STEP,VAL,M,NFN)
C
C      — BY WILLIAM T. WYATT, JR., 1978.
C
C  USING THE METHOD OF CONJUGATE GRADIENTS, THIS SUBROUTINE SEARCHES FOR
C  THE MINIMUM OF THE SCALAR FUNCTION FN, GIVEN A STARTING POINT X.
C  X IS A VECTOR OF LENGTH M. AN ELEMENT OF X IS NOT ALTERED
C  DURING THE SEARCH IF THE CORRESPONDING ELEMENT OF TOL IS NON-
C  POSITIVE. OTHERWISE, THE SEARCH CONTINUES UNTIL THE FUNCTION DOES
C  NOT DECREASE WHEN X IS CHANGED BY AS MUCH AS TOL*STEP, WHERE THE
C  LARGEST ELEMENT IN STEP IS UNITY.
C
C  THE SEARCH MAY BE ABORTED AFTER ABOUT NFN EVALUATIONS OF THE
C  FUNCTION FN IF NFN>0, OR AFTER -NFN GRADIENT EVALUATIONS IF
C  NFN<0.
C
C  THE FUNCTION FN MUST BE DECLARED EXTERNAL IN THE CALLING PROGRAM.
C  X, TOL, M, AND NFN MUST BE DEFINED WHEN THIS SUBROUTINE IS
C  CALLED. THE SUBROUTINE RETURNS THE MINIMUM LOCATION IN X, THE
C  MINIMUM FUNCTION VALUE IN VAL, AND THE NUMBER OF FUNCTION
C  EVALUATIONS IN ABS(NFN). NFN IS RETURNED NEGATIVE IF THE SEARCH
C  IS ABORTED AS DESCRIBED ABOVE. THE ARRAYS B, G, XOLD, AND
C  STEP OF LENGTH M ARE USED FOR INTERMEDIATE RESULTS. TOL AND M
C  ARE RETURNED UNCHANGED.
C
C  THE PROGRAM CALLS THE SUBROUTINE QUAD TO LOCATE A MINIMUM ALONG A
C  GIVEN DIRECTION.
C
C  AN ELEMENT OF X MAY BE COMPELLED TO REMAIN POSITIVE DURING THE
C  SEARCH, BY USING THE TWO STATEMENTS (MARKED WITH "CCCCC") IN THE
C  PROGRAM BELOW:
C
C      TOL(I)=-TOL(I)
C      GO TO 5
C
C  THE METHOD ESTIMATES THE FUNCTION GRADIENT BY FINITE DIFFERENCES OVER
C  AN INTERVAL TOL*SLASH. SLASH HAS BEEN SET TO 0.01 IN A DATA
C  STATEMENT. ROUND OFF ERRORS WILL CAUSE POOR ESTIMATES FOR THE
C  GRADIENT IF TOL IS TOO SMALL OR IF MACHINE PRECISION IS
C  INSUFFICIENT. (DOUBLE PRECISION IS RECOMMENDED FOR COMPUTERS WITH
C  DEFAULT SHORT PRECISION WORDS.)
C
C      DIMENSION X(M),TOL(M),B(M),G(M),XOLD(M),STEP(M)
C      DATA SLASH /0.01/
C
C  INITIALIZE GRADIENT AND DIRECTION ARRAYS AND OTHER QUANTITIES.
C      MAXFN=NFN
C      NFN=0
C      IPASS=0
5    CONTINUE
      DO 10 I=1,M
        B(I)=0.0
10     G(I)=1.0
      VAL=FN(X)
      NFN=NFN+1
C
C
C  MINIMIZATION LOOP BEGINS HERE. CHECK FOR MAX FN EVALUATIONS.
100  CONTINUE

```

## APPENDIX B

```

IPASS=IPASS+1
IF(IPASS.GT.-MAXFN.AND.MAXFN.LT.0) GO TO 900
IF(MFN.GT.MAXFN.AND.MAXFN.GT.0) GO TO 900
C
C FIRST, MOVE X TO XOLD.
SUMOLD=0.0
DO 110 I=1,M
XOLD(I)=X(I)
110 SUMOLD=SUMOLD+G(I)**2
IF(SUMOLD.EQ.0.0) GO TO 5
FNOLD=VAL
C NEXT, GET GRADIENT AND NEW SEARCH DIRECTION.
SUM=0.0
DO 120 I=1,M
G(I)=0.0
IF(TOL(I).LE.0.0) GO TO 120
X(I)=XOLD(I)+SLASH*TOL(I)
VAL=FN(X)
NFN=NFN+1
X(I)=XOLD(I)
G(I)=(VAL-FNOLD)/SLASH
120 SUM=SUM+G(I)**2
SUM=SUM/SUMOLD
DO 130 I=1,M
B(I)=-G(I)+SUM*B(I)
130 STEP(I)=B(I)
C
C SCALE STEP SO EACH ELEMENT IS .LE. 1.0.
SAVE=0.0
DO 140 I=1,M
TEMP=ABS(STEP(I))
IF(TEMP.GT.SAVE) SAVE=TEMP
140 CONTINUE
IF(SAVE.NE.0.0) SAVE=1.0/SAVE
C
C TAKE TRIAL STEP.
DO 150 I=1,M
STEP(I)=STEP(I)*TOL(I)*SAVE
C LOCKUP PARAMETER TENDING TO ZERO.
IF(STEP(I).GE.0.0.OR.XOLD(I).GT.TOL(I)) GO TO 150
CCCCC TOL(I)=-TOL(I)
CCCCC GO TO 5
150 X(I)=XOLD(I)+STEP(I)
VAL=FN(X)
NFN=NFN+1
IF(VAL.GE.FNOLD) GO TO 910
C MINIMUM IMPROVED. DO SEARCH FOR MINIMUM.
CALL QUAD(FN,M,OLDVAL,VAL,XOLD,STEP,X,NFN)
CCCCC PRINT 97,VAL
97 FORMAT(' NEW VAL=',E20.8)
GO TO 100
C
C
C FINISHED.
900 NFN=-NFN
DO 905 I=1,M
905 TOL(I)=ABS(TOL(I))
RETURN
910 CONTINUE
IF(IPASS.GT.5) GO TO 915

```

## APPENDIX B

```
C TRY THROWING OUT A BAD PARAMETER IF IN EARLY STAGES OF MINIMIZATION.
DO 914 I=1,M
  IF(STEP(I).EQ.0.0) GO TO 914
  SAVE=STEP(I)
  STEP(I)=0.0
  X(I)=XOLD(I)
  VAL=FN(X)
  NFN=NFN+1
  IF(VAL.GE.FNOLD) GO TO 913
  CALL QUAD(FN,M,OLDVAL,VAL,XOLD,STEP,X,NFN)
  B(I)=0.0
  G(I)=0.0
  GO TO 100
913 STEP(I)=SAVE
  X(I)=XOLD(I)+STEP(I)
914 CONTINUE
915 CONTINUE
C RESTORE X AND VAL.
VAL=FNOLD
DO 920 I=1,M
  TOL(I)=ABS(TOL(I))
920 X(I)=XOLD(I)
  RETURN
END
```

# APPENDIX B

SUBROUTINE QUAD(FN,MPARAM,FNOLD,VAL,XOLD,STEP,X,NFN)

```

C
C
C      -- BY WILLIAM T. WYATT, JR., 1970.
C
C  THIS SUBROUTINE FINDS THE MINIMUM OF THE FUNCTION FN IN THE DIRECTION
C  STEP, GIVEN FNOLD=FN(XOLD), VAL=FN(X), X=XOLD+STEP, AND MPARAM (THE
C  LENGTH OF VECTORS X, XOLD, AND STEP). A NECESSARY CONDITION IS THAT
C  VAL < FNOLD. NFN, A COUNTER FOR FUNCTION CALLS, IS INCREMENTED FOR
C  EACH EVALUATION OF FN. THE SUBROUTINE RETURNS A MINIMUM VAL AND
C  ARGUMENT X SUCH THAT VAL=FN(X), AND STEP SUCH THAT STEP=X-XOLD.
C
C  THE ALGORITHM USES QUADRATIC INTERPOLATION ACCELERATED BY A LOGARITH-
C  MIC BISECTION-TYPE SEARCH.
C
C      DIMENSION XOLD(MPARAM),STEP(MPARAM),X(MPARAM)
C  ICOUNT LIMITS THE NUMBER OF FUNCTION EVALUATIONS TO A NUMBER
C  CONVENIENT FOR THIS APPLICATION. THE USER MAY CHANGE IT.
C      ICOUNT=AMAX1(3.0,SQRT(FLOAT(MPARAM)))
C      IC=0
C      SA=0.
C      SB=1.0
C      FA=FNOLD
C      FB=VAL
C  LOOK FOR A FC.GE.FB.
10  SC=SB+10.0
    DO 20 I=1,MPARAM
      X(I)=XOLD(I)+STEP(I)*SC
    CONTINUE
20  FC=FN(X)
    NFN=NFN+1
    IF(FC.GE.FB) GO TO 100
C  TRY AGAIN.
    FA=FB
    FB=FC
    SA=SB
    SB=SC
    GO TO 10
C  BEGIN MODIFIED QUADRATIC INTERPOLATION FOR MINIMUM.
100 CONTINUE
    IC=IC+1
    IF(IC.GT.ICOUNT) GO TO 170
    TEMP=(SC-SB)/(SB-SA)
    IF(TEMP.GT.4.0) GO TO 110
    IF(TEMP.LT.0.25) GO TO 120
    IF(FA.EQ.FB.OR.FB.EQ.FC) GO TO 170
    CA=((FA-FB)/(SA-SB)-(FB-FC)/(SB-SC))/(SA-SC)
    IF(CA.EQ.0.0) GO TO 110
    CB=(FA-FB)/(SA-SB)-CA*(SA+SB)
    SX=-CB/(2.0*CA)
    GO TO 130
110 CONTINUE
C  EITHER CONVERGING VERY WELL, OR POORLY. USE LOGARITHMIC SEARCH.
    TEMP=SQRT(TEMP)-1.0
    SX=SB+(SB-SA)*TEMP
    GO TO 130
120 TEMP=SQRT(1.0/TEMP)-1.0
    SX=SB-(SC-SB)*TEMP
130 CONTINUE
    IF(SX.EQ.SB.OR.SX.LE.SA.OR.SX.GE.SC) GO TO 170

```

# APPENDIX B

C EVALUATE FUNCTION AT INTERPOLATED POINT.

DO 135 I=1,MPARAM  
X(I)=XOLD(I)+STEP(I)\*SX  
135 CONTINUE  
FX=FN(X)  
NFN=NFN+1

IF(FX.LT.FB) GO TO 150

C NOT NEW MINIMUM.

IF(SX.GT.SB) GO TO 140

SA=SX  
FA=FX  
GO TO 100

140 SC=SX  
FC=FX  
GO TO 100

150 CONTINUE

C IS NEW MINIMUM.

IF(SX.LT.SB) GO TO 160

SA=SB  
FA=FB  
SB=SX  
FB=FX  
GO TO 100

160 SC=SB  
FC=FB  
SB=SX  
FB=FX  
GO TO 100

170 CONTINUE  
VAL=FB

DO 180 I=1,MPARAM  
STEP(I)=STEP(I)\*SB  
X(I)=XOLD(I)+STEP(I)

180 CONTINUE

C FINISHED.

RETURN

END

# DISTRIBUTION

ADMINISTRATOR  
DEFENSE DOCUMENTATION CENTER  
ATTN DDC-TCA (12 COPIES)  
CAMERON STATION, BUILDING 5  
ALEXANDRIA, VA 22314

COMMANDER  
US ARMY RSCH & STD GP (EUR)  
ATTN LTC JAMES M. KENNEDY, JR.  
CHIEF, PHYSICS & MATH BRANCH  
FFO NEW YORK 09510

COMMANDER  
US ARMY ARMAMENT MATERIEL  
READINESS COMMAND  
ATTN DRSAR-LEP-L, TECHNICAL LIBRARY  
ROCK ISLAND, IL 61299

COMMANDER  
US ARMY MISSILE & MUNITIONS  
CENTER & SCHOOL  
ATTN ATSK-CTD-F  
REDSTONE ARSENAL, AL 35809

DIRECTOR  
US ARMY MATERIEL SYSTEMS  
ANALYSIS ACTIVITY  
ATTN DREBY-MP  
ATTN DREBY-PO  
ABERDEEN PROVING GROUND, MD 21005

DIRECTOR  
US ARMY BALLISTIC RESEARCH LABORATORY  
ATTN DRDAR-TSB-S (STIMFO)  
ATTN DREAR-AM, W. VANANTWERP  
ATTN DRETE-EL  
ATTN DRDAR-BLS  
ABERDEEN PROVING GROUND, MD 21005

U.S. ARMY ELECTRONICS TECHNOLOGY  
AND DEVICES LABORATORY  
ATTN DELET-DD  
FORT MONMOUTH, NJ 07703

TEXAS INSTRUMENTS, INC.  
P.O. BOX 226015  
ATTN FRANK POBLENZ,  
DALLAS, TX 75266

TELEDYNE BROWN ENGINEERING  
CUMMINGS RESEARCH PARK  
ATTN DR. MELVIN L. PRINCE, MS-44  
HUNTSVILLE, AL 35807

ENGINEERING SOCIETIES LIBRARY  
345 EAST 47TH STREET  
ATTN ACQUISITIONS DEPARTMENT  
NEW YORK, NY 10017

DIRECTOR  
ARMED FORCES RADIOBIOLOGY RESEARCH  
INSTITUTE  
DEFENSE NUCLEAR AGENCY  
NATIONAL NAVAL MEDICAL CENTER  
ATTN RESEARCH PROGRAM COORDINATING  
OFFICER  
BETHESDA, MD 20014

ASSISTANT TO THE SECRETARY OF DEFENSE  
ATOMIC ENERGY  
ATTN EXECUTIVE ASSISTANT  
WASHINGTON, DC 20301

DIRECTOR  
DEFENSE ADVANCED RSCH PROJ AGENCY  
ARCHITECT BUILDING  
ATTN TIO  
1400 WILSON BLVD.  
ARLINGTON, VA 22209

DIRECTOR  
DEFENSE CIVIL PREPAREDNESS AGENCY  
ASSISTANT DIRECTOR FOR RESEARCH  
ATTN ADMIN OFFICER  
ATTN RE (EO)  
ATTN PO (SE)  
WASHINGTON, DC 20301

DEFENSE COMMUNICATIONS ENGINEERING  
CENTER  
ATTN CODE R720, C. STANSBERRY  
ATTN CODE R123, TECH LIB  
ATTN CODE R400  
1860 WISHLIE AVENUE  
RESTON, VA 22090

DIRECTOR  
DEFENSE COMMUNICATIONS AGENCY  
ATTN CCTC C312  
ATTN CODE C313  
WASHINGTON, DC 20305

DIRECTOR  
DEFENSE INTELLIGENCE AGENCY  
ATTN RDS-3A  
ATTN RDS-3A4, POMPOONIO PLAZA  
WASHINGTON, DC 20301

DIRECTOR  
DEFENSE NUCLEAR AGENCY  
ATTN RATN  
ATTN DOST  
ATTN RAEV  
ATTN TITL  
ATTN STVL  
ATTN VLIS  
WASHINGTON, DC 20305

COMMANDER  
FIELD COMMAND  
DEFENSE NUCLEAR AGENCY  
ATTN FCPR  
ATTN FCSFM, J. SMITH  
ATTN FCLMC  
KIRTLAND AFB, NM 87115

DIRECTOR  
INTERSERVICE NUCLEAR WEAPONS SCHOOL  
ATTN TTV  
KIRTLAND AFB, NM 87115

JOINT CHIEFS OF STAFF  
ATTN J-3  
WASHINGTON, DC 20301

DIRECTOR  
JOINT STRATEGIC TARGET PLANNING  
STAFF, JCS  
OFFUTT AFB  
ATTN JSAS  
ATTN JPST  
ATTN NRI-STIMFO LIBRARY  
OMAHA, NE 68113

CHIEF  
LIVERMORE DIVISION  
FIELD COMMAND DNA  
DEPARTMENT OF DEFENSE  
LAWRENCE LIVERMORE LABORATORY  
P.O. BOX 808  
ATTN FCPRL  
LIVERMORE, CA 94550

NATIONAL COMMUNICATIONS SYSTEM  
OFFICE OF THE MANAGER  
DEPARTMENT OF DEFENSE  
ATTN NCS-TS, CHARLES D. BOBSON  
WASHINGTON, DC 20305

DIRECTOR  
NATIONAL SECURITY AGENCY  
DEPARTMENT OF DEFENSE  
ATTN R-52, O. VAN GUNTER  
ATTN S232, D. VINCENT  
FT. MEADE, MD 20755

UNDER SECY OF DEF FOR RSCH & ENGRG  
DEPARTMENT OF DEFENSE  
ATTN G. BARGE  
ATTN S6SS (OS)  
WASHINGTON DC 20301

COMMANDER  
BMD SYSTEM COMMAND  
DEPARTMENT OF THE ARMY  
P.O. BOX 1500  
ATTN BMDSC-AOLIB  
HUNTSVILLE, AL 35807

COMMANDER  
ERADCOM TECHNICAL SUPPORT ACTIVITY  
DEPARTMENT OF THE ARMY  
ATTN DELCS-K, A COHEN  
ATTN DELET-IR, E. HUNTER  
FORT MONMOUTH, NJ 07703

COMMANDER  
US ARMY ARMOR CENTER  
ATTN TECHNICAL LIBRARY  
FORT KNOX, KY 40121

COMMANDER  
US ARMY COMM-ELEC ENGRG INSTAL  
AGENCY  
ATTN CCC-PRSO-S  
ATTN CCC-CEB-SBS  
FT HUCHUCA, AZ 85613

COMMANDER  
US ARMY COMMUNICATIONS COMMAND  
COMBAT DEVELOPMENT DIVISION  
ATTN ATSI-CD-MD  
FT. HUCHUCA, AZ 85613



DISTRIBUTION (Cont'd)

CHIEF  
US ARMY COMMUNICATIONS SYS AGENCY  
ATTN COM-RO-T COM-AD-SV  
FORT MONMOUTH, NJ 07703

PROJECT OFFICER  
US ARMY COMMUNICATIONS RES &  
DEV COMMAND  
ATTN DRCFM-ATC  
ATTN DRCFM-TDS-BSI  
FORT MONMOUTH, NJ 07703

DIVISION ENGINEER  
US ARMY ENGINEER DIV HUNTSVILLE  
P.O. BOX 1600, WEST STATION  
ATTN ENDED-SR  
ATTN A. T. BOLT  
HUNTSVILLE, AL 35807

US ARMY INTEL THREAT ANALYSIS  
DETACHMENT  
ROOM 2201, BLDG A  
ARLINGTON HALL STATION  
ATTN RM 2200, BLDG A  
ARLINGTON, VA 22212

COMMANDER  
US ARMY INTELLIGENCE & SEC CMD  
ARLINGTON HALL STATION  
4000 ARLINGTON BLVD  
ATTN TECHNICAL LIBRARY  
ATTN TECH INFO FAC  
ARLINGTON, VA 22212

COMMANDER  
US ARMY MISSILE RESEARCH  
& DEVELOPMENT COMMAND  
ATTN DRCFM-PE-EA, WALLACE O. WAGNER  
ATTN DRCFM-PE-EG, WILLIAM B. JOHNSON  
ATTN DRDMI-TBD  
ATTN DRDMI-EAA  
REDSTONE ARSENAL, AL 35809

US ARMY NUCLEAR & CHEMICAL AGENCY  
7500 BACKLICK ROAD  
BUILDING 2073  
ATTN COL A. LOWRY  
ATTN DR. J. BERBERET  
SPRINGFIELD, VA 22150

COMMANDER  
US ARMY TEST AND EVALUATION COMMAND  
ATTN DRSTE-PA  
ABERDEEN PROVING GROUND, MD 21005

COMMANDER  
US ARMY TRAINING AND  
DOCTRINE COMMAND  
ATTN ATORI-OP-SW  
FORT MONROE, VA 23651

COMMANDER  
WHITE SANDS MISSILE RANGE  
DEPARTMENT OF THE ARMY  
ATTN STEWS-TE-AM, J. OKUMA  
WHITE SANDS MISSILE RANGE, NM 88002

OFFICER-IN-CHARGE  
CIVIL ENGINEERING LABORATORY  
NAVAL CONSTRUCTION BATTALION CENTER  
ATTN CODE LOSA (LIBRARY)  
ATTN CODE LOSA  
PORT HUENEME, CA 93041

COMMANDER  
NAVAL AIR SYSTEMS COMMAND  
ATTN AIR-350F  
WASHINGTON, DC 21360

COMMANDER  
NAVAL ELECTRONIC SYSTEMS COMMAND  
ATTN PME 117-215  
WASHINGTON, DC 20360

COMMANDER  
NAVAL OCEAN SYSTEMS CENTER  
ATTN CODE 015, C. FLETCHER  
ATTN RESEARCH LIBRARY  
ATTN CODE 7240, S. W. LICHTMAN  
SAN DIEGO, CA 92152

COMMANDING OFFICER  
NAVAL ORDNANCE STATION  
ATTN STANDARDIZATION DIV  
INDIAN HEAD, MD 20640

SUPERINTENDENT (CODE 1424)  
NAVAL POSTGRADUATE SCHOOL  
ATTN CODE 1424  
MONTEREY, CA 93940

DIRECTOR  
NAVAL RESEARCH LABORATORY  
ATTN CODE 4104, EMANUEL L. BRANCATO  
ATTN CODE 2627, DORIS R. POLEN  
ATTN CODE 6623, RICHARD L. STATLER  
ATTN CODE 6624  
WASHINGTON, DC 20375

COMMANDER  
NAVAL SHIP ENGINEERING CENTER  
DEPARTMENT OF THE NAVY  
ATTN CODE 6174D2, EDWARD F. DUFFY  
WASHINGTON, DC 20362

COMMANDER  
NAVAL SURFACE WEAPONS CENTER  
ATTN CODE F32, EDWIN R. RATHBURN  
ATTN L. LIBELLO, CODE WR43  
ATTN CODE WAS1RH, NM 130-108  
WHITE OAK, SILVER SPRING, MD 20910

COMMANDER  
NAVAL SURFACE WEAPONS CENTER  
DAHLGREN LABORATORY  
ATTN CODE DF-36  
DAHLGREN, VA 22448

COMMANDER  
NAVAL WEAPONS CENTER  
ATTN CODE 533, TECH LIB  
CHINA LAKE, CA 93555

COMMANDING OFFICER  
NAVAL WEAPONS EVALUATION FACILITY  
KIRTLAND AIR FORCE BASE  
ATTN CODE AT-6  
ALBUQUERQUE, NM 87117

OFFICE OF NAVAL RESEARCH  
ATTN CODE 427  
ARLINGTON, VA 22217

DIRECTOR  
STRATEGIC SYSTEMS PROJECT OFFICE  
NAVY DEPARTMENT  
ATTN NSP-2701, JOHN W. FITZBERGER  
ATTN NSP-2342, RICHARD L. COLEMAN  
ATTN NSP-43, TECH LIB  
ATTN NSP-27334  
ATTN NSP-230, D. GOLD  
WASHINGTON, DC 20376

COMMANDER  
AERONAUTICAL SYSTEMS DIVISION, AFSC  
ATTN ASD-YH-EK  
ATTN EMFTV  
WRIGHT-PATTERSON AFB, OH 45333

AIR FORCE TECHNICAL APPLICATIONS  
CENTER  
ATTN TFS, M. SCHNEIDER  
PATRICK AFB, FL 32925

AF WEAPONS LABORATORY, AFSC  
ATTN WTN  
ATTN WT  
ATTN EL, CARL E. BAUM,  
ATTN ELKT  
ATTN SUL  
ATTN CA  
ATTN ELA, J. P. CASTILLO  
ATTN ELP  
ATTN ELT, W. PAGE  
ATTN WES  
KIRTLAND AFB, NM 87117

DIRECTOR  
AIR UNIVERSITY LIBRARY  
DEPARTMENT OF THE AIR FORCE  
ATTN AUL-LSE-70-250  
MAXWELL AFB, AL 36112

HEADQUARTERS  
ELECTRONIC SYSTEMS DEVISION/YSEA  
DEPARTMENT OF THE AIR FORCE  
ATTN YSEA  
WANSBOM AFB, MA 01731

COMMANDER  
FOREIGN TECHNOLOGY DIVISION, AFSC  
ATTN NICO LIBRARY  
ATTN ETDP, S. L. BALLARD  
WRIGHT-PATTERSON AFB, OH 45433

COMMANDER  
OGDEN ALC/MNEDEE  
DEPARTMENT OF THE AIR FORCE  
ATTN OO-ALC/NEETH, P. W. BERTHEL  
ATTN MNEDE, LEO KIDMAN  
ATTN MAJ R. BLACKBURN  
HILL AFB, UT 84406

DISTRIBUTION (Cont'd)

COMMANDER  
ROME AIR DEVELOPMENT CENTER AFSC  
ATTN TSLD  
GRIFFISS AFB, NY 13441

COMMANDER  
SACRAMENTO AIR LOGISTICS CENTER  
DEPARTMENT OF THE AIR FORCE  
ATTN NMCRS, H. A. PELMASTRO  
ATTN NMIRA, J. W. DEMES  
ATTN NMARM, F. R. SPEAR  
MCCLLELLAN AFB, CA 95652

SAMSO/IN  
AIR FORCE SYSTEMS COMMAND  
POST OFFICE BOX 92960  
WORLDWAY POSTAL CENTER  
(INTELLIGENCE)  
ATTN IND  
LOS ANGELES, CA 90009

SAMSO/MN  
AIR FORCE SYSTEMS COMMAND  
(MINUTEMAN)  
ATTN MNMH, MAJ M. BARAN  
ATTN MNMH, CAPT R. I. LAWRENCE  
NORTON AFB, CA 92409

SAMSO/YA  
AIR FORCE SYSTEMS COMMAND  
POST OFFICE BOX 92960  
WORLDWAY POSTAL CENTER  
ATTN YAPC  
LOS ANGELES, CA 90009

STRATEGIC AIR COMMAND/XPFS  
ATTN NRI-STINFO LIBRARY  
ATTN DEL  
ATTN GARNET E. MATEKE  
ATTN XPFS, MAJ BRIAN G. STEPHEN  
OFFUTT AFB, NE 68113

DEPARTMENT OF ENERGY  
ALBUQUERQUE OPERATIONS OFFICE  
P.O. BOX 5400  
ATTN DOC CON FOR TECH LIBRARY  
ATTN OPERATIONAL SAFETY DIV  
ALBUQUERQUE, NM 87115

UNIVERSITY OF CALIFORNIA  
LAWRENCE LIVERMORE LABORATORY  
P.O. BOX 808  
ATTN DOC CON FOR TECHNICAL  
INFORMATION DEPT  
ATTN DOC CON FOR L-06, T. DONICH  
ATTN DOC CON FOR L-545, D. HEEKER  
ATTN DOC CON FOR L-156, E. MILLER  
ATTN DOC CON FOR L-10, H. KRUGER  
ATTN DOC CON FOR H. S. CABAYAN  
LIVERMORE, CA 94550

LOS ALAMOS SCIENTIFIC LABORATORY  
P.O. BOX 1663  
ATTN DOC CON FOR BRUCE W. NOEL  
ATTN DOC CON FOR CLARENCE BENTON  
LOS ALAMOS, NM 87545

SANDIA LABORATORIES  
P.O. BOX 5800  
ATTN DOW CON FOR C. W. VITTOR  
ATTN DOW CON FOR R. L. PARKER  
ATTN DOC CON FOR ELMER F. HARTMAN  
ALBUQUERQUE, NM 87115

CENTRAL INTELLIGENCE AGENCY  
ATTN RD/SI, RM 5G48, HQ BLDG  
FOR OSI/WED/WNB  
WASHINGTON, DC 20505

ADMINISTRATOR  
DEFENSE ELECTRIC POWER ADMIN  
DEPARTMENT OF THE INTERIOR  
INTERIOR SOUTH BLDG, 312  
ATTN L. O'NEILL  
WASHINGTON, DC 20240

DEPARTMENT OF TRANSPORTATION  
FEDERAL AVIATION ADMINISTRATION  
HEADQUARTERS SEC DIV, ASE-300  
800 INDEPENDENCE AVENUE, SW  
ATTN SEC DIV ASE-300  
WASHINGTON, DC 20591

AEROSPACE CORPORATION  
P.O. BOX 92957  
ATTN C. B. PEARLSTON  
ATTN IRVING M. GARFUNKEL  
ATTN JULIAN REINHEDMER  
ATTN LIBRARY  
ATTN CHARLES GREENHOW  
LOS ANGELES, CA 90009

AGBARIAN ASSOCIATES  
250 NORTH WASH STREET  
ATTN LIBRARY  
EL SEGUNDO, CA 90245

AVCO RESEARCH & SYSTEMS GROUP  
201 LOWELL STREET  
ATTN W. LEPSEVICH  
WILMINGTON, MA 01887

BATTELLE MEMORIAL INSTITUTE  
505 KING AVENUE  
ATTN ROBERT H. BALZER  
ATTN EUGENE R. LEACH  
COLUMBUS, OH 43201

BDM CORPORATION  
7915 JONES BRANCH DRIVE  
ATTN CORPORATE LIBRARY  
MCLEAN, VA 22101

BDM CORPORATION  
P.O. BOX 9274  
ALBUQUERQUE INTERNATIONAL  
ATTN LIB  
ALBUQUERQUE, NM 87119

BENDIX CORPORATION, THE  
RESEARCH LABORATORIES DIVISION  
BENDIX CENTER  
ATTN MAX FRANK  
SOUTHFIELD, MI 48075

BENDIX CORPORATION  
NAVIGATION AND CONTROL GROUP  
ATTN DEPT 6401  
TETERBORO, NJ 07608

BOEING COMPANY  
P.O. BOX 3707  
ATTN HOWARD W. WICKLEIN  
ATTN D. E. ISBELL  
ATTN DAVID KEMLE  
ATTN B. C. HANRAHAN  
ATTN KENT TECH LIB  
SEATTLE, WA 98124

BOGE-ALLEN AND HAMILTON, INC.  
106 APPLE STREET  
ATTN E. J. CHRISNER  
ATTN TECH LIB  
TINTON FALLS, NJ 07724

BURROUGHS CORPORATION  
FEDERAL AND SPECIAL SYSTEMS GROUP  
CENTRAL AVE AND ROUTE 252  
P.O. BOX 517  
ATTN ANGELO J. MAURIELLO  
PAOLI, PA 19301

CALSPAN CORPORATION  
P.O. BOX 400  
ATTN TECH LIBRARY  
BUFFALO, NY 14225

CHARLES STARK DRAPER LABORATORY INC.  
555 TECHNOLOGY SQUARE  
ATTN KENNETH FERTIG  
ATTN TIC MS 74  
CAMBRIDGE, MA 02139

CINCINNATI ELECTRONICS CORPORATION  
2630 GLENDALE-HILFORD ROAD  
ATTN LOIS HAMMOND  
CINCINNATI, OH 45241

COMPUTER SCIENCES CORPORATION  
6565 ARLINGTON BLVD  
ATTN RAMONA BRIGGS  
FALLS CHURCH, VA 22046

COMPUTER SCIENCES CORPORATION  
1400 SAN MATEO BLVD, SE  
ATTN RICHARD E. DICKHAUT  
ATTN ALVIN SCHIFF  
ALBUQUERQUE, NM 87108

CONTROL DATA CORPORATION  
P.O. BOX 0  
ATTN JACK MEEHAN  
MINNEAPOLIS, MN 55440

CUTLER-HAMMER, INC.  
AII DIVISION  
COMAC ROAD  
ATTN EDWARD KARPEN  
DEER PARK, NY 11729

DIXONWOOD INDUSTRIES, INC  
1009 BRANDSBURY DRIVE, SE  
ATTN TECH LIB  
ATTN L. WAYNE DAVIS  
ALBUQUERQUE, NM 87106

DISTRIBUTION (Cont'd)

DIKEWOOD INDUSTRIES, INC.  
1100 GLENDON AVENUE  
ATTN K. LEE  
LOS ANGELES, CA 90024

E-SYSTEMS, INC  
GREENVILLE DIVISION  
P.O. BOX 1056  
ATTN JOLETA MOORE  
GREENVILLE, TX 75401

EFFECTS TECHNOLOGY, INC.  
5383 HOLLISTER AVENUE  
ATTN S. CLOW  
SANTA BARBARA, CA 93111

EG&G WASHINGTON ANALYTICAL  
SERVICES CENTER, INC.  
P.O. BOX 10218  
ATTN C. GILES  
ALBUQUERQUE, NM 87114

EDISON NUCLEAR COMPANY, INC.  
RESEARCH AND TECHNOLOGY CENTER  
2955 GEORGE WASHINGTON WAY  
ATTN DR. A. W. TRIVELPIECE  
RICHLAND, WA 99352

FAIRCHILD CAMERA AND INSTRUMENT CORP  
464 ELLIS STREET  
ATTN SEC CON FOR DAVID K. MYERS  
MOUNTAIN VIEW, CA 94040

FORD AEROSPACE & COMMUNICATIONS CORP  
3939 FABIAN WAY  
ATTN TECHNICAL LIBRARY  
PALO ALTO, CA 94303

FORD AEROSPACE & COMMUNICATIONS  
OPERATIONS  
FORD & JAMBOROE ROADS  
ATTN KEN C. ATTINGER  
ATTN E. R. PONCELET, JR.  
NEWPORT BEACH, CA 92663

FRANKLIN INSTITUTE, THE  
20TH STREET AND PARKWAY  
ATTN NAMIE H. THOMPSON  
PHILADELPHIA, PA 19103

GENERAL DYNAMICS CORP  
ELECTRONICS DIVISION  
P.O. BOX 81125  
ATTN RSCN LIB  
SAN DIEGO, CA 92138

GENERAL DYNAMICS CORPORATION  
INTER-DIVISION RESEARCH LIBRARY  
KEARNY MESA  
P.O. BOX 80847  
ATTN RESEARCH LIBRARY  
SAN DIEGO, CA 98123

GENERAL ELECTRIC CO.-TEMPO  
CENTER FOR ADVANCED STUDIES  
816 STATE STREET (TO DRAWER QQ)  
ATTN DASAC  
ATTN ROYDEN R. RUTHERFORD  
ATTN WILLIAM MCNAMEE  
SANTA BARBARA, CA 93102

GENERAL ELECTRIC COMPANY  
AEROSPACE ELECTRONICS SYSTEMS  
FRENCH ROAD  
ATTN CHARLES M. HEMISON  
UTICA, NY 13503

GENERAL ELECTRIC COMPANY  
P.O. BOX 5000  
ATTN TECH LIB  
BINGHAMTON, NY 13902

GENERAL ELECTRIC CO.-TEMPO  
ALEXANDRIA OFFICE  
HUNTINGTON BUILDING, SUITE 300  
2560 HUNTINGTON AVENUE  
ATTN DASAC  
ALEXANDRIA, VA 22303

GENERAL RESEARCH CORPORATION  
SANTA BARBARA  
P.O. BOX 6770  
ATTN TECH INFO OFFICE  
SANTA BARBARA, CA 93111

GEORGIA INSTITUTE OF TECHNOLOGY  
GEORGIA TECH RESEARCH INSTITUTE  
ATTN R. CURRY  
ATLANTA, GA 30332

GEORGIA INSTITUTE OF TECHNOLOGY  
OFFICE OF CONTRACT ADMINISTRATION  
ATTN RES & SEC COORD FOR HUGH DENNY  
ATLANTA, GA 30332

GRUMMAN AEROSPACE CORPORATION  
SOUTH OYSTER BAY ROAD  
ATTN L-01 35  
BETHPAGE, NY 11714

GTE SYLVANIA INC.  
ELECTRONICS SYSTEMS GRP-EASTERN DIV  
77 A STREET  
ATTN CHARLES A. THORNHILL, LIBRARIAN  
ATTN LEONARD L. BLAISDELL  
NEEDHAM, MA 02194

GTE SYLVANIA, INC.  
189 B STREET  
ATTN CHARLES H. RAMSBOTTOM  
ATTN DAVID D. FLOOD  
ATTN EMIL P. MOTCHOK  
ATTN H & V GROUP, MARIO A. NUREPORA  
ATTN J. WALDRON  
NEEDHAM HEIGHTS, MA 02194

HARRIS CORPORATION  
HARRIS SEMICONDUCTOR DIVISION  
P.O. BOX 883  
ATTN V PRES & MGR PRGMS DIV  
MELBOURNE, FL 32901

HAZELTINE CORPORATION  
PULASKI ROAD  
ATTN TECH INFO CTR, M. WAITE  
GREENLAWN, NY 11740

HONEYWELL INCORPORATED  
AVIONICS DIVISION  
2600 RIDGEWAY PARKWAY  
ATTN S&RC LIB  
ATTN RONALD R. JOHNSON  
MINNEAPOLIS, MN 55413

HONEYWELL INCORPORATED  
AVIONICS DIVISION  
13350 U.S. HIGHWAY 19 NORTH  
ATTN M.S 725-5, STACEY H. GRAFF  
ATTN W. E STEWART  
ST. PETERSBURG, FL 33733

HUGHES AIRCRAFT COMPANY  
CENTINELA AND TEALE  
ATTN JOHN B. SINGLETARY  
ATTN CTDC 6/E110  
ATTN KENNETH R. WALKER  
CULVER CITY, CA 90230

IIT RESEARCH INSTITUTE  
ELECTROMAG COMPATABILITY ANAL CTR  
NORTH SEVERN  
ATTN ACOAT  
ANNAPOLIS, MD 21402

IIT RESEARCH INSTITUTE  
10 WEST 35TH STREET  
ATTN IRVING M. MINDEL  
ATTN JACK E. BRIDGES  
CHICAGO, IL 60616

INSTITUTE FOR DEFENSE ANALYSES  
400 ARMY-NAVY DRIVE  
ATTN TECH INFO SERVICES  
ARLINGTON, VA 22202

INTL TEL & TELEGRAPH CORPORATION  
500 WASHINGTON AVENUE  
ATTN TECHNICAL LIBRARY  
ATTN ALEXANDER T. RICHARDSON  
MUTLEY, NJ 07110

IRT CORPORATION  
P.O. BOX 81087  
ATTN C. B. WILLIAMS  
ATTN DENNIS SWIFT  
SAN DIEGO, CA 92138

JAYCOR  
SANTA BARBARA FACILITY  
P.O. BOX 2008  
ATTN W. A. MADASKY  
SANTA BARBARA, CA 93120

JAYCOR  
1401 CAMINO DEL MAR  
ATTN ERIC P. WENASAS  
ATTN RALPH H. STARR  
DEL MAR, CA 92014

JAYCOR  
205 S WHITING STREET, SUITE 500  
ATTN LIB  
ALEXANDRIA, VA 22304

DISTRIBUTION (Cont'd)

KAMAN SCIENCES CORPORATION  
1500 GARDEN OF THE GODS ROAD  
ATTN ALBERT P. BRIDGES  
ATTN W. FOSTER RICH  
ATTN WALTER E. WARE  
ATTN FRANK H. SHELTON  
ATTN JERRY I. LUBELL  
ATTN PHIL TRACY  
ATTN WERNER STARK  
COLORADO SPRINGS, CO 80907

LITTON SYSTEMS, INC.  
DATA SYSTEMS DIVISION  
8000 WOODLEY AVENUE  
ATTN EMC GP  
ATTN M848-61  
VAN NUYS, CA 91409

LITTON SYSTEMS, INC.  
AMECOM DIVISION  
5115 CALVERT ROAD  
ATTN J. SKAGGS  
COLLEGE PARK, MD 20740

LOCKHEED MISSILES AND SPACE  
COMPANY, INC.  
P.O. BOX 504  
ATTN L. ROSSI  
ATTN SAMUEL I. TAINUTY  
ATTN H. E. THAYN  
ATTN GEORGE F. HEATH  
ATTN BENJAMIN T. KIMURA  
SUNNYVALE, CA 94086

LOCKHEED MISSILES AND SPACE  
COMPANY, INC.  
3251 HANOVER STREET  
ATTN TECH INFO CTR D/COLL  
PALO ALTO, CA 94304

M.I.T. LINCOLN LABORATORY  
P.O. BOX 73  
ATTN LEONA LOUGHLIN  
LEXINGTON, MA 02173

MARTIN MARIETTA CORPORATION  
ORLANDO DIVISION  
P.O. BOX 5837  
ATTN MONA C. GRIFFITH  
ORLANDO, FL 32805

MCDONNELL DOUGLAS CORPORATION  
POST OFFICE BOX 516  
ATTN TOM ENDER  
ST. LOUIS, MO 63166

MCDONNELL DOUGLAS CORPORATION  
5301 BOLSA AVENUE  
ATTN STANLEY SCHNEIDER  
ATTN TECH LIBRARY SERVICES  
HUNTINGTON BEACH, CA 92647

MISSION RESEARCH CORPORATION  
P.O. DRAWER 719  
ATTN EMP GROUP  
ATTN WILLIAM C. HART  
ATTN C. LONGMIRE  
SANTA BARBARA, CA 93102

MISSION RESEARCH CORPORATION  
EM SYSTEM APPLICATIONS DIVISION  
1400 SAN MATEO BLVD, SE, SUITE A  
ATTN DAVID E. MEREWETHER  
ATTN L. N. MCCORMICK  
ALBUQUERQUE, NM 87108

MISSION RESEARCH CORPORATION  
-SAN DIEGO  
P.O. BOX 1209  
ATTN V. A. J. VAN LINT  
LA JOLLA, CA 92038

MITRE CORPORATION, THE  
P.O. BOX 208  
ATTN M. F. FITZGERALD  
BEDFORD, MA 01730

NORDEN SYSTEMS, INC.  
HELEN STREET  
ATTN TECHNICAL LIBRARY  
NORWALK, CT 06856

NORTHROP RESEARCH TECHNOLOGY CENTER  
ONE RESEARCH PARK  
ATTN LIBRARY  
PALOS VERDES PENN, CA 90274

NORTHROP CORPORATION  
ELECTRONIC DIVISION  
2301 WEST 120TH STREET  
ATTN LEW SMITH  
ATTN RAD EFFECTS GRP  
HAWTHORNE, CA 90250

PHYSICS INTERNATIONAL COMPANY  
2700 MERCED STREET  
ATTN DOC CON  
SAN LEANDRO, CA 94577

R.&D ASSOCIATED  
P.O. BOX 9695  
ATTN S. CLAY ROGERS  
ATTN RICHARD R. SCHAEFER  
ATTN DOC CON  
ATTN M. GROVER  
ATTN C. MACDONALD  
MARINA DEL REY, CA 90291

R&D ASSOCIATES  
1401 WILSON BLVD  
SUITE 500  
ATTN J. BOMBARDT  
ARLINGTON, VA 22209

RAND CORPORATION  
1700 MAIN STREET  
ATTN LIB-D  
ATTN W. SOLLFREY  
SANTA MONICA, CA 90406

RAYTHEON COMPANY  
HARTWELL ROAD  
ATTN GAJANAN H. JOSI  
BEDFORD, MA 01730

RAYTHEON COMPANY  
528 BOSTON POST ROAD  
ATTN HAROLD L. FLEISCHER  
SUDBURY, MA 01776

RCA CORPORATION  
GOVERNMENT SYSTEMS DIVISION  
ASTRO ELECTRONICS  
P.O. BOX 800, LOCUST CORNER  
EAST WINDSOR TOWNSHIP  
PRINCETON, NJ 08540

RCA CORPORATION  
DAVID SARNOFF RESEARCH CENTER  
P.O. BOX 432  
ATTN SECURITY DEPT, L. MINICH  
PRINCETON, NJ 08540

RCA CORPORATION  
CAMDEN COMPLEX  
FRONT & COOPER STREETS  
ATTN OLIVE WHITEHEAD  
ATTN R. W. TOSTROM  
CAMDEN, NJ 08012

ROCKWELL INTERNATIONAL CORPORATION  
P.O. BOX 3105  
ATTN N. J. RUDIE  
ATTN J. L. MONROE  
ATTN V. J. MICHEL  
ATTN D/243-068, 031-CA31  
ANAHEIM, CA 92803

ROCKWELL INTERNATIONAL CORPORATION  
SPACE DIVISION  
12214 SOUTH LAKEWOOD BOULEVARD  
ATTN B. E. WHITE  
DOWNEY, CA 90241

ROCKWELL INTERNATIONAL CORPORATION  
815 LAPAHN STREET  
ATTN E-1, DIV TIC (BAOB)  
EL SEGUNDO, CA 90245

ROCKWELL INTERNATIONAL CORPORATION  
P.O. BOX 369  
ATTN F. A. SHAW  
CLEARFIELD, UT 84015

SANDERS ASSOCIATES, INC.  
95 CANAL STREET  
ATTN 1-6270, R. G. DESPATHY, SR P E  
NASHUA, NH 03060

SCIENCE APPLICATIONS, INC.  
P.O. BOX 277  
ATTN FREDERICK M. TESCHE  
BERKELEY, CA 94701

SCIENCE APPLICATIONS, INC.  
P.O. BOX 2351  
ATTN R. PARKINSON  
LA JOLLA, CA 92038

SCIENCE APPLICATIONS, INC.  
HUNTSVILLE DIVISION  
2109 W. CLINTON AVENUE  
SUITE 700  
ATTN NOEL R. BYRN  
HUNTSVILLE, AL 35805

SCIENCE APPLICATIONS, INC.  
8400 WESTPARK DRIVE  
ATTN WILLIAM L. CHADSEY  
MCLEAN, VA 22101

DISTRIBUTION (Cont'd)

SINGER COMPANY  
ATTN: SECURITY MANAGER  
FOR TECH INFO CTR  
1150 MC BRIDE AVENUE  
LITTLE FALLS, NJ 07424

SPERRY RAND CORPORATION  
SPERRY MICROWAVE ELECTRONICS  
P.O. BOX 4648  
ATTN MARGARET CORT  
CLEARWATER, FL 33518

SPERRY RAND CORPORATION  
SPERRY DIVISION  
MARCUS AVENUE  
ATTN TECH LIB  
GREAT NECK, NY 11020

SPERRY RAND CORPORATION  
SPERRY FLIGHT SYSTEMS  
P.O. BOX 21111  
ATTN D. ANDREW SCHOW  
PHOENIX, AZ 85036

SPIRE CORPORATION  
P.O. BOX D  
ATTN JOHN R. UGLIN  
ATTN ROGER G. LITTLE  
BEDFORD, MA 01730

SRI INTERNATIONAL  
333 RAVENSWOOD AVENUE  
ATTN ARTHUR LEE WHITSON  
MENLO PARK, CA 94025

SYSTEMS, SCIENCE AND SOFTWARE, INC.  
P.O. BOX 1620  
ATTN ANDREW R. WILSON  
LA JOLLA, CA 92038

TEXAS INSTRUMENTS, INC.  
P.O. BOX 6015  
ATTN TECH LIB  
ATTN DONALD J. MANUS  
DALLAS, TX 75265

TRW DEFENSE & SPACE SYS GROUP  
ONE SPACE PARK  
ATTN O. E. ADAMS  
ATTN R. K. PLEBUCH  
ATTN L. R. MAGNOLIA  
ATTN H. H. HOLLOWAY  
ATTN W. GARGARO  
REDONDO BEACH, CA 90278

TEXAS TECH UNIVERSITY  
P.O. BOX 5404 NORTH COLLEGE STATION  
ATTN TRAVIS L. SIMPSON  
LUBBOCK, TX 79417

UNITED TECHNOLOGIES CORP  
HAMILTON STANDARD DIVISION  
BRADLEY INTERNATIONAL AIRPORT  
ATTN CHIEF ELEC DESIGN  
WINDSOR LOCKS, CT 06069

WESTINGHOUSE ELECTRIC CORPORATION  
ADVANCED ENERGY SYSTEMS DIV  
P.O. BOX 10864  
ATTN TECH LIB  
PITTSBURGH, PA 15236

US ARMY ELECTRONICS RESEARCH  
& DEVELOPMENT COMMAND  
ATTN TECHNICAL DIRECTOR, DRDEL-CT

HARRY DIAMOND LABORATORIES  
ATTN CO/TO/TSO/DIVISION DIRECTORS  
ATTN RECORD COPY, 81200  
ATTN HDL LIBRARY 81100 (3 COPIES)  
ATTN HDL LIBRARY (WOODBIDGE) 81100  
ATTN TECHNICAL REPORTS BRANCH, 81300  
ATTN CHAIRMAN, EDITORIAL COMMITTEE  
ATTN CHIEF, 21000  
ATTN CHIEF, 22000  
ATTN CHIEF, 22100 (3 COPIES)  
ATTN CHIEF, 22300  
ATTN CHIEF, 22800  
ATTN CHIEF, 22900  
ATTN CHIEF, 13300  
ATTN CHIEF, 21100 (3 COPIES)  
ATTN CHIEF, 21200  
ATTN CHIEF, 21300 (5 COPIES)  
ATTN CHIEF, 21400 (2 COPIES)  
ATTN CHIEF, 21500  
ATTN BALICKI, P. W., 20240  
ATTN WIDENITZ, P. M., 20240  
ATTN TALLERICO, A., 47400  
ATTN BIXBY, R., 22900  
ATTN WEATT, W. T., 21300 (20 COPIES)